JCI The Journal of Clinical Investigation

RNF4 sustains Myc-driven tumorigenesis by facilitating DNA replication

Joonyoung Her, … , Haiyan Zheng, Samuel F. Bunting

J Clin Invest. 2024. https://doi.org/10.1172/JCI167419.

Research In-Press Preview Genetics Oncology

Graphical abstract

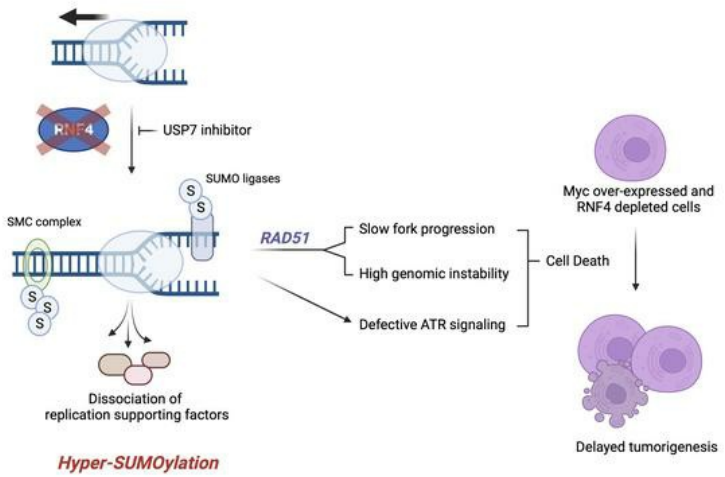

RNF4 sustains Myc-driven tumorigenesis by facilitating DNA replication

Joonyoung Her[1], Haiyan Zheng[2], and Samuel F. Bunting[1, *]

1. Department of Molecular Biology and Biochemistry, Rutgers, The State University of New Jersey, Piscataway, NJ, USA.

2. Biological Mass Spectrometry Facility, Rutgers, The State University of New Jersey, Piscataway, NJ, USA.

* Corresponding author:
Samuel F. Bunting
Center for Advanced Biotechnology and Medicine, Rutgers, The State University of New Jersey,
679 Hoes Lane West, Piscataway, NJ 08854, USA.
848.445.9894
bunting@cabm.rutgers.edu

Conflict-of-interest statement: The authors have declared that no conflict of interest exists.

Abstract

The mammalian SUMO-targeted E3 Ubiquitin Ligase, *Rnf4*, has been reported to act as a regulator of DNA repair, but the importance of RNF4 as a tumor suppressor has not been tested. Using a conditional-knockout mouse model, we deleted *Rnf4* in the B cell lineage to test the importance of RNF4 for growth of somatic cells. Although *Rnf4* conditional-knockout B cells exhibited substantial genomic instability, *Rnf4* deletion caused no increase in tumor susceptibility. In contrast, *Rnf4* deletion extended the healthy lifespan of mice expressing an oncogenic c-*myc* transgene. *Rnf4* activity is essential for normal DNA replication, and in its absence, there was a failure in ATR-CHK1 signaling of replication stress. Factors that normally mediate replication fork stability, including members of the Fanconi Anemia gene family and the helicases, PIF1 and RECQL5, showed reduced accumulation at replication forks in the absence of RNF4. RNF4 deficiency also resulted in an accumulation of hyper-SUMOylated proteins in chromatin, including members of the SMC5/6 complex, which contributes to replication failure by a mechanism dependent on RAD51. These findings indicate that RNF4, which shows increased expression in multiple human tumor types, is a potential target for anti-cancer therapy, especially in tumors expressing c-*myc.*

Introduction

Healthy cell growth requires post-translational modification of proteins by addition of ubiquitin (Ub) or the Small Ubiquitin-like Modifier (SUMO) (1, 2). Ubiquitination and SUMOylation regulate almost every aspect of cellular physiology by modifying the function and stability of cellular proteins. DNA replication and repair are examples of the importance of SUMOylation and ubiquitination, which act in coordination to ensure productive outcomes in each case (3, 4).

In mammalian cells, RNF4 (RING Finger Protein 4), is a key SUMO-targeted E3 ubiquitin ligase (STUbL), which has a central importance in linking protein regulation by SUMOylation and ubiquitination. RNF4 contains four SUMO-Interacting Motifs (SIMs), which target the protein to SUMOylated substrates. The E3 ubiquitin ligase activity of homodimeric RNF4 subsequently transfers Ub from one of a number of different E2 conjugating enzymes to the substrate (5). RNF4 is known to target the PML:RARA fusion protein that is frequently found in acute promyelocytic leukemia (APL) (6). In response to arsenic trioxide treatment, PML undergoes increased SUMOylation, making it an improved target for RNF4 STUbL activity, leading to degradation of the PML-RARA fusion protein and successful treatment outcomes even without use of conventional cytotoxic chemotherapy (7).

In addition to regulation of PML stability, RNF4 is implicated in a range of cellular processes. Several studies, using siRNA knockdown, mutant cell lines, or DT40 cells, reported defects in the cellular response to DNA damage after loss of RNF4 activity (8-12). In particular, efficiency of the homologous recombination (HR) pathway was reported to be reduced in si*RNF4* cells, as a

consequence of a failure to load RPA and RAD51 at resected DNA double-strand breaks (13, 14). RNF4 also promotes normal chromosome segregation, based on its ability to remove toxic DNA-protein crosslinks that interfere with mitosis (15). Mutations affecting other components of the HR machinery, such as *BRCA1* or *BRCA2*, increase the rate of genetic mutations, leading to substantially increased tumor risk (16). Around 6% of primary cancer cases are estimated to be affected by HR deficiency (17), and identifying these cases is of substantial importance for treatment, because HR-deficient cancers show greatly increased sensitivity to Poly(ADP-Ribose) Polymerase (PARP) inhibitors and platinum-based cross-linking agents (18). Human *RNF4* mutations that might predispose affected individuals to cancer have not yet been reported, however, and the importance of *RNF4* as a tumor suppressor is unknown.

A challenge to evaluating the importance of RNF4 as a tumor suppressor is the lack of suitable animal models to test whether loss of RNF4 increases the risk of malignant cell growth. Homozygous deletion of the mouse *Rnf4* gene causes embryonic lethality prior to E15 (19). We now report the use of a conditional-knockout *Rnf4* mouse model to test the importance of *Rnf4* for DNA repair, and to evaluate how *Rnf4* deficiency contributes to tumor susceptibility. We find that deletion of *Rnf4* causes genomic instability and reduced cellular viability. These phenotypes of *Rnf4* deficiency are an outcome of defective DNA replication, and can be partially rescued by inhibiting the ubiquitin isopeptidase, USP7. The increased genomic instability of *Rnf4*-deficient cells does not lead to a higher frequency of malignant neoplasms, however, even on a p53-deficient background. *Rnf4* deficiency instead significantly delayed the rate of tumor formation in a mouse model of c-*myc* overexpression, indicating that *Rnf4* contributes to the growth of

incipient tumors. These results demonstrate that RNF4 is an essential factor for DNA replication and a potential novel target for anti-cancer therapy.

Results

Rnf4 deletion causes genomic instability and cell death in primary B cells

To test the importance of RNF4 for growth of somatic cells, we first attempted to rescue embryonic lethality in *Rnf4*$^{-/-}$ mice by crossing to *Trp53*$^{-/-}$ or *Trp53bp1*$^{-/-}$ mouse lines. Co-deletion of p53 or 53BP1 in these lines rescues embryonic lethality in *Brca1*$^{\Delta 11/\Delta 11}$ mice (20), but we were not able to obtain any viable *Rnf4*$^{-/-}$ pups by this approach, indicating that *Rnf4* has an indispensable role in normal embryonic development (Supplemental Table 1). We therefore generated a novel, conditional *Rnf4*^{fl} allele by introducing LoxP sites around *Rnf4* exon 6 (Figure 1A). *Rnf4*$^{fl/fl}$ mice were crossed to *CD19-Cre* animals to delete *Rnf4* selectively in the B lymphocyte lineage (21). The spleens of these *Rnf4* conditional-knockout (*Rnf4*$^{\Delta/\Delta}$) mice showed a near-normal population of mature B220^{+} B cells, but RNF4 was undetectable in protein lysates from these cells (Figure 1B and C). *Rnf4*$^{\Delta/\Delta}$ B cells showed a substantially increased proportion of high-molecular-weight SUMOylated species, consistent with the known role of RNF4 in ensuring turnover of SUMOylated proteins (6).

B cells lacking RNF4 showed clear signs of cell stress after 48 hrs of in vitro culture, with stabilization of p53, and increased cleavage of caspase-3 (Figure 1C). Phosphorylation of KAP1, and H2AX was also increased (Figure 1D), indicating activation of ATM and ATR after DNA damage (22). Markers of DNA damage and apoptosis became increasingly apparent after three days of in vitro B cell culture, indicating an underlying stress that became more acute after a longer period of B cell activation. Analysis of metaphase chromosomes revealed a significant

increase in chromosome aberrations in *Rnf4*$^{\Delta/\Delta}$ B cells (Figure 1E). This increase was apparent after 24 hrs of in vitro culture, and reached an even greater level after 48 hrs of culture. There was additionally an increase in the frequency of sister chromatid exchanges in *Rnf4*$^{\Delta/\Delta}$ cells, indicating increased use of HR-mediated DNA repair (Supplemental Figure 1A). *Rnf4*$^{\Delta/\Delta}$ B cells also showed a disrupted cell cycle, with a slightly reduced proportion of S phase cells, and an increase in the proportion of cells in G2 phase (Figure 1F).

Consistent with the increased induction of apoptotic markers, the majority of *Rnf4*$^{\Delta/\Delta}$ B cells became non-viable after three days in culture (Figure 1G). Cell death and increased genomic instability was only observed in homozygous *Rnf4*$^{\Delta/\Delta}$ cells, and not in heterozygotes (Figure 1H and I). Although p53 is clearly stabilized in *Rnf4*$^{\Delta/\Delta}$ cells (Figure 1C), deletion of *Trp53* only partially rescued cell viability and had no significant impact on chromosome instability (Supplemental Figure 1 B and C). RNF4 therefore plays an essential role for ensuring the viability of proliferating primary B cells, and in its absence, cells undergo apoptosis by a combination of p53-mediated and p53-independent processes.

Rnf4-knockout cells show defects in DNA replication

To evaluate the importance of RNF4 for DNA repair, we challenged *Rnf4*$^{\Delta/\Delta}$ cells with a range of compounds that cause DNA damage of various kinds (Supplemental Figure 2A). These agents included olaparib, a PARP inhibitor that produces DNA double-strand breaks in replicating cells; ionizing radiation (IR), which produces DNA double-strand breaks in all phases of the cell cycle; the DNA crosslinking agents, mitomycin C (MMC), and cisplatin (CDDP); and methyl

methanesulfonate (MMS), a DNA alkylating agent. In each case, *Rnf4*$^{\Delta/\Delta}$ cells showed an increase in chromosome instability after treatment, but the increase in *Rnf4*$^{\Delta/\Delta}$ cells was not significantly greater than that observed in WT cells after subtracting the rate of chromosome breaks and rearrangements in the untreated condition (Supplemental Figure 2B). A high frequency of chromosome aberrations was observed after olaparib or cisplatin treatment of *Brca1*$^{\Delta 11/\Delta 11}$ cells, which express a hypomorphic form of BRCA1, and are HR-deficient (23) (Figure 2A). In contrast, *Rnf4*$^{\Delta/\Delta}$ cells showed only a very mild increase in the frequency of chromosome breaks and rearrangements after treatment with olaparib or cisplatin, despite having a higher rate of chromosome instability in the absence of drug treatment. The relatively mild sensitivity of *Rnf4*$^{\Delta/\Delta}$ cells after treatments to induce DNA damage suggests that defects in additional cellular processes may contribute to the genomic instability and poor growth of these cells.

The proliferation and viability of *Rnf4*$^{\Delta/\Delta}$ cells was significantly impacted by treatment with either MMS, or the DNA polymerase inhibitor, aphidicolin (APH) (Figure 2B, and Supplemental Figure 2C and D). These agents also induced strong caspase-3 cleavage in *Rnf4*$^{\Delta/\Delta}$ cells (Figure 2C). MMS produces cytotoxicity through production of single-stranded DNA breaks and by inhibition of DNA replication (24-26). Although we did not detect an increase in single-strand breaks in *Rnf4*$^{\Delta/\Delta}$ cells (Supplemental Figure 2E), we observed that *Rnf4*$^{\Delta/\Delta}$ cells were hypersensitive to the replication inhibitors hydroxyurea, aphidicolin, and gemcitabine (Figure 2D). *Rnf4*$^{\Delta/\Delta}$ cells also showed an increase in 53BP1 G1 nuclear bodies, a hallmark of cells that are encountering problems with DNA replication (Figure 2E) (27, 28). *Rnf4*$^{\Delta/\Delta}$ cells consistently incorporated lower levels of the deoxythymidine analog, EdU, indicating a lower rate of DNA

replication (Figure 2F). To directly measure the activity of individual replication forks, we performed a DNA combing analysis after pulsing cells with CldU and IdU, which revealed that *Rnf4*$^{\Delta/\Delta}$ cells showed a significant reduction in replication fork velocity (Figure 2G). *Rnf4*$^{\Delta/\Delta}$ cells also showed reduced stability of newly-replicated DNA after hydroxyurea treatment (Figure 2H). ATR-mediated CHK1 phosphorylation is essential for signaling the presence of replication stress (29), but phosphorylation of CHK1 was defective after induction of replication stress in the absence of RNF4 (Figure 2I). Although replication forks in *Rnf4*$^{\Delta/\Delta}$ cells appeared to restart normally after HU treatment (Supplemental Figure 2F), and showed only marginal levels of fork asymmetry (Supplemental Figure 2G), the reduction in replication fork progression induced by MMS treatment in WT cells is not observed in RNF4-conditional-knockout cells (Supplemental Figure 2H). A failure to adequately signal replication stress therefore correlates with reduced replication efficiency in *Rnf4*$^{\Delta/\Delta}$ cells.

Replication defects and cell death in Rnf4$^{\Delta/\Delta}$ *cells are a consequence of deregulated SUMOylation*

Transduction of *Rnf4*$^{\Delta/\Delta}$ B cells with a construct expressing WT RNF4 resulted in a rescue of cell viability and EdU uptake (Fig 3A-B). This effect was not seen with RNF4 constructs containing mutations in the E3 ubiquitin ligase active site, or in the SUMO-interaction motifs. The STUbL activity of RNF4 is therefore essential for normal cell viability. To test whether the defective DNA replication, genomic instability, and cell death observed in *Rnf4*$^{\Delta/\Delta}$ cells are specifically caused by the accumulation of high-MW SUMOylated proteins, we used inhibitors of Ubiquitin Specific Protease 7 (USP7), a ubiquitin isopeptidase that removes ubiquitin from SUMOylated

substrates (30). Short-term treatment with USP7 inhibitor produced an increase in the amount of ubiquitination of SUMOylated proteins (Supplemental Figure 3), indicating that other cellular E3 ubiquitin ligases target SUMOylated proteins at some level in the absence of RNF4. Continuous treatment with the USP7 inhibitors, P22077 or P5091, substantially reversed the accumulation of SUMOylated proteins in *Rnf4*$^{\Delta/\Delta}$ cells, presumably by stabilizing ubiquitin chains on those proteins to enable proteasomal targeting (Figure 3C). This reduction in the quantity of SUMOylated proteins was associated with a rescue in the speed of replication forks in *Rnf4*$^{\Delta/\Delta}$ cells (Figure 3D), reduced cell death (Figure 3E and F), and a reduction in the frequency of chromosome aberrations (Figure 3G and H). These results suggest that the slow replication forks, genomic instability, and increased cell death observed in *Rnf4*$^{\Delta/\Delta}$ cells arise because of a failure to properly degrade SUMOylated proteins. Inhibition of SUMOylation by 2-D08, which blocks transfer of SUMO from UBC9 to potential substrates (31), or by ML-792, which inhibits the SUMO-Activating enzyme, SAE1/2 (32), also produced a partial rescue of chromosome instability and cell death in *Rnf4*$^{\Delta/\Delta}$ cells (Figure 3I and J), showing that accumulation of poly-SUMOylated proteins in *Rnf4*$^{\Delta/\Delta}$ cells is causative of reduced cell viability.

Rnf4 deletion leads to defective recruitment of proteins required for replication stress responses

To identify changes in cellular protein expression that might account for the genomic instability and reduced viability of *Rnf4*$^{\Delta/\Delta}$ cells, we performed quantitative isobaric labeling mass spectrometry with resting B cells (Day 0) and cells that were stimulated to divide in vitro for 48 hrs (Day 2). In resting B cells, there was no substantial difference in protein expression between WT and *Rnf4*$^{\Delta/\Delta}$ cells (Figure 4A, Supplemental Table 2). After activation of B cells and the

initiation of cell division, there were substantial changes in protein abundance in both the WT and *Rnf4*$^{\Delta/\Delta}$ samples (Figure 4B). Activated *Rnf4*$^{\Delta/\Delta}$ B cells showed a modest, but statistically-significant increase in the abundance of 455 proteins encompassing a broad range of protein classes (Supplemental Table 3, Supplemental Figure 4A and B). Increases in the abundance of several of these proteins were validated by Western blotting (Figure 4C). The broad changes in protein expression in *Rnf4*$^{\Delta/\Delta}$ B cells are consistent with previous proteomic studies, which revealed that RNF4 targets a wide range of substrates (33, 34).

As *Rnf4*$^{\Delta/\Delta}$ cells appear to have specific problems with DNA replication, we next used iPOND (isolation of Proteins On Nascent DNA) (35) to identify proteins with altered abundance at replication forks (Supplemental Table 4). Protein enrichment analysis on candidate proteins that showed substantially altered abundance at replication forks in *Rnf4*$^{\Delta/\Delta}$ cells revealed a cluster of proteins around FANCD2 (Supplemental Figure 4C), including Fanconi Anemia family proteins with known functions in ensuring stable replication (36). Several of these proteins show reduced abundance at replication forks in *Rnf4*$^{\Delta/\Delta}$ cells (Figure 4D), potentially accounting for the reduced replication efficiency seen in the absence of RNF4. The helicases PIF1 and RECQL5, which are required for DNA replication through difficult substrates (37, 38), also show diminished abundance in iPOND samples from RNF4-deficient cells. These results demonstrate that *Rnf4*$^{\Delta/\Delta}$ cells show a deficiency in recruitment of proteins necessary for replication fork stability and progression.

Rnf4$^{\Delta/\Delta}$ cells accumulate poly-SUMOylated proteins in chromatin (Supplemental Figure 4D). We performed immunoprecipitation of SUMO2/3 on chromatin samples from WT and *Rnf4*$^{\Delta/\Delta}$ cells,

to attempt to identify hyper-SUMOylated chromatin proteins in *Rnf4*$^{\Delta/\Delta}$ samples, which might contribute to defective replication fork progression. Mass spectrometry revealed a set of proteins with two clusters including proteins involved in regulation of SUMOylation, which are known targets of RNF4 (34), and several members of the SMC5/6 complex (Supplemental Table 5, Supplemental Figure 4E and F). The SMC5/6 complex is regulated by SUMOylation, and contributes to replication fork stability and regulation of recombination (39). SUMOylated SMC5 and SMC6 were significantly enriched in chromatin from *Rnf4*$^{\Delta/\Delta}$ cells relative to WT (Figure 4E). Three Non-SMC Element (NSMCE) subunits of the SMC5/6 complex were additionally present at increased abundance in SUMO2/3 immunoprecipitated proteins (Figure 4F). The SMC5/6 complex therefore shows significant deregulation and hyper-SUMOylation in chromatin of *Rnf4*$^{\Delta/\Delta}$ cells, which may contribute to deficiencies in responding to replication stress.

Cell death and genomic instability in RNF4-deficient cells are dependent on RAD51

The SMC5/6 complex is known to prevent the accumulation of toxic recombination intermediates that appear at stalled replication forks (39, 40). We observed that knockdown of *RNF4* using multiple different siRNAs in U2OS EJ-DR reporter cells caused an increase in the rate of HR-mediated repair of DNA double-strand breaks (Supplemental Figure 5A). Ionizing radiation-induced foci of RAD51 formed normally in the nuclei of *Rnf4*$^{\Delta/\Delta}$ B cells (Supplemental Figure 5B). To test whether a potential increase in DNA recombination in RNF4-deficient cells might contribute to apoptosis and defective replication, we used the RAD51 inhibitors, RI-1 and B02 (41, 42). At high concentrations, these agents can block formation of ionizing-radiation

induced RAD51 foci, and reduce HR efficiency in reporter assays (Supplemental Figure 5C and D). Treatment with lower doses did not have a measurable impact on the cell cycle of WT cells (Supplemental Figure 5E), but substantially improved the growth of RNF4-deficient B cells (Fig 5A-H). RAD51 inhibition significantly reduced the p53 activation and caspase-3 cleavage normally observed in *Rnf4*$^{\Delta/\Delta}$ cells, reduced the frequency of chromosome aberrations, and improved cell proliferation and viability. Improved growth of *Rnf4*$^{\Delta/\Delta}$ cells after RAD51 inhibition was associated with a rescue of replication fork velocity (Figure 5I). RAD51 did not show an increased abundance at replication forks in iPOND data sets from *Rnf4*$^{\Delta/\Delta}$ cells, however, nor is the overall abundance or level of ubiquitination of RAD51 substantially changed (Supplemental Figure 5F-H). RAD51-mediated toxicity may arise because of dysregulation of some other RNF4 target, as USP7 inhibition also reduced the hyper-recombinogenic phenotype of siRNF4-treated cells (Supplemental Figure 5I). Targeting other proteins involved in homologous recombination did not achieve a similar rescue of the phenotypes of RNF4 deficiency as was achieved with RAD51 inhibition. In particular, deletion of either *Brca1* or *Brca2* did not result in an improvement in the proliferation, viability, or genomic integrity of *Rnf4*$^{\Delta/\Delta}$ cells (Supplemental Figure 6A-F).

Deletion of Rnf4 delays tumor formation in a c-myc cancer model

As B cells from *Rnf4*-conditional-knockout mice showed substantial genomic instability (Figure 1E), we performed a longitudinal study to determine if *Rnf4*-conditional-knockout mice are at increased risk of cancer. Despite elevated genomic instability in *Rnf4*$^{\Delta/\Delta}$ B cells grown in culture, there was no difference in tumor susceptibility caused by deletion of *Rnf4* in the B cell lineage

(Figure 6A). The overall survival of conditional knockout and control mice also showed no significant difference (Supplemental Figure 7A). Tumor susceptibility in *Brca1*- and *Brca2*-deficient mice is more apparent in a p53-hemizygous background (43-45). We therefore crossed *Rnf4*-conditional-knockout mice to a $Trp53^{+/-}$ background, to test whether loss of RNF4 causes tumor outgrowth in cells lacking normal expression of p53. We observed that *Rnf4* deficiency did not accelerate tumor formation, even on a $Trp53^{+/-}$ background (Figure 6B), or affect the overall survival rate of $Trp53^{+/-}$ mice (Supplemental Figure 7B). As in the control group, $Rnf4^{\Delta/\Delta}$;$Trp53^{+/-}$ animals developed tumors characteristic of p53 loss-of-function, with a large proportion of thymomas (46). Finally, we tested whether *Rnf4* deficiency causes accelerated tumor formation in E*μ-myc* mice, a transgenic model for overexpression of the oncogene, c-*myc*, in B cells (47). As expected, mice carrying the E*μ-myc* transgene had a very high incidence of B cell lymphoma with a median survival rate of 123 days (Figure 6C). In contrast, mice expressing E*μ-myc* with conditional deletion of *Rnf4* in the B cell lineage showed a significant delay in tumor formation, with a median tumor-free survival of 215 days. The overall lifespan of E*μ-myc;*$Rnf4^{\Delta/\Delta}$ mice showed an equivalent extension (Supplemental Figure 7C). These studies show that *Rnf4* deletion does not predispose mice to tumor formation, and loss of *Rnf4* delays the onset of tumors in cells with c-*myc* overexpression.

We considered whether defects in DNA replication might limit the growth of incipient *myc*-dependent malignancies in mice carrying the E*μ-myc* transgene. Consistent with the well-known ability of c-*myc* to induce cellular proliferation, we observed EdU uptake by freshly-isolated E*μ-myc*;$Rnf4^{+/+}$ and E*μ-myc;*$Rnf4^{\Delta/\Delta}$ B cells, whereas WT and $Rnf4^{\Delta/\Delta}$ B cells showed almost no EdU incorporation (Supplemental Figure 7D). A proportion of E*μ-myc* splenic B cells are therefore

dividing, even in the absence of any exogenous mitogenic stimulus. As was the case in *Rnf4*$^{\Delta/\Delta}$ cells, we measured an increased frequency of chromosome aberrations in E*μ-myc;Rnf4*$^{\Delta/\Delta}$ B cells relative to E*μ-myc*;*Rnf4*$^{+/+}$ cells (Fig 6D). E*μ-myc;Rnf4*$^{\Delta/\Delta}$ B cells also showed a significantly reduced ability to proliferate in culture as compared to E*μ-myc*;*Rnf4*$^{+/+}$ cells (Figure 6E). We tested the effect of knocking down RNF4 on the growth of U2OS cells with a stably-integrated, doxycycline-inducible c-*myc* construct (48). After knockdown of *RNF4*, these U2OS-iMYC cells showed significantly reduced proliferation compared to cells transfected with control siRNA (Figure 6F). In E*μ-myc*-transgenic cells, deletion of *Rnf4* also led to reduced replication fork velocity, higher levels of γ-H2AX in S phase, and an increased number of 53BP1 G1 nuclear bodies (Figure 6G and H, and Supplemental Figure 7E). These results are consistent with the concept that the increased propensity of *myc*-transgenic cells to proliferate makes them acutely sensitive to loss of RNF4, which is required for normal DNA replication.

To consider whether *RNF4* expression might impact the growth of tumors in humans, we analyzed survival of B cell acute lymphoblastic leukemia patients studied as part of the NCI TARGET Phase II initiative. Patients with tumors expressing high levels of *RNF4* had significantly worse survival outcomes than those expressing normal levels of *RNF4* (Fig 6I). Elevated *RNF4* expression is a feature of several tumor types in TCGA data sets (Supplemental Figure 7F), and high *RNF4* expression correlates with poor survival in multiple tumor types, including breast adenocarcinoma, and lung adenocarcinoma (Supplemental Figure 7G-H). These findings suggest that RNF4 may have a general role in supporting tumor outgrowth, by facilitating DNA replication in malignant cells.

Discussion

Our observation that deletion of *Rnf4* does not lead to malignancy in B lymphocytes, even in the absence of p53, is potentially surprising considering the high rate of genomic instability observed in RNF4-deficient cells. Mice with deletions in known DNA repair genes, such as *Brca1* or *Brca2*, show tumor susceptibility, especially on a p53-deficient background (43, 45). The rate of chromosome instability in untreated $Rnf4^{\Delta/\Delta}$ B cells is significantly higher than that in $Brca1^{\Delta 11/\Delta 11}$ B cells (Fig 2A), and yet no tumor susceptibility was observed in *Rnf4* conditional-knockout mice. This outcome is potentially similar to the situation with cells lacking RAD51, the central mediator of HR (49). Repression of *RAD51* expression leads to accumulation of chromatid and chromosome breaks (50), but *RAD51* mutations do not correlate strongly with cancer incidence (51). Mouse knockout studies have shown that loss of RAD51 causes a complete block in cellular proliferation (52, 53), therefore it is likely that cancer cells cannot survive in the absence of RAD51. Based on our results, we propose that a similar effect is caused by loss of RNF4, in that knockout cells show chromosome instability, but are also unable to replicate and divide normally, leading to cell death instead of malignancy.

We find that the block on cell growth caused by conditional inactivation of *Rnf4* is so strong as to limit the outgrowth of c-*myc* dependent lymphomas. Tumors driven by *myc* activity are dependent on SUMOylation, and SUMO regulators are upregulated by *myc* overexpression (54). Our work further underscores the importance of SUMO regulation for tumor cell growth, and reveals the importance of RNF4 in this pathway. The dependence of incipient tumor cells from E*μ*-*myc* mice on RNF4 for survival and tumor outgrowth is an example of 'non-oncogene

addiction' (55). Increased proliferative signaling arising from *myc* overexpression leads to rapid DNA replication, which can only be sustained if RNF4 is available to ensure appropriate ubiquitination in replicating chromatin domains. A similar effect is seen with loss of ATR and CHK1, which signal the presence of DNA replication stress, including that induced by oncogene expression (29). CHK1 inhibition compromises the growth of tumors overexpressing oncogenic Ras or Myc, and tumor formation is significantly reduced in E*μ-myc* mice expressing mutant ATR (56, 57).

Several studies in mammalian cells have supported a role for RNF4 in regulation of DNA replication. In ATR-deficient cells, RNF4 promotes SLX4-mediated cleavage of replication forks, leading to fork collapse and the appearance of DNA double-strand breaks (58). RNF4 knockdown also reduces the ability of replication forks to restart after persistent replication stress, based on the ability of RNF4 to ubiquitinate BLM helicase (59). Another recent study identified RNF4 as the factor responsible for removal of the ZAPP-TOP2a-PICH complex from replication forks (33, 60). This finding is consistent with earlier studies, which showed that RNF4 targets trapped TOP1- and TOP2-cleavage complexes for proteasomal degradation (61, 62). Several studies have identified PARP1 as a target of the E3 ubiquitin ligase activity of RNF4 (63, 64). PARP1 is active at replication forks, and the cytotoxic effect of PARP inhibitors is partially dependent on their ability to trap PARP1 on chromatin, creating a barrier to replication fork progression (65). Although we observed modest increases in the abundance of PARP1, TOP2A, and TOP2B in whole cell extracts from *Rnf4*$^{\Delta/\Delta}$ cells (Figure 4B and C), we did not observe significant changes in these factors in iPOND-MS studies of proteins at active replication forks. We did find reductions in the abundance of FANCD2, FANCI, and FANCM at

366 replication forks in RNF4-deficient cells (Fig 4D). Each of these factors is known to function in
367 ensuring replication fork progression and stability (66-68). The helicases PIF1 and RECQL5,
368 which are required for replication through challenging substrates such as G quadruplexes and
369 transcription-replication conflict sites, are also present at reduced abundance at replication forks
370 of *Rnf4*$^{\Delta/\Delta}$ cells (37, 38).
371
372 Work from the Fernandez-Capetillo lab has supported a model in which chromatin around active
373 DNA replication forks is marked by high levels of SUMOylation and low levels of ubiquitination
374 (69). According to this model, chromatin outside of active replicating regions is marked by lower
375 levels of SUMOylation, and high levels of ubiquitination. Disruption of the normal balance of
376 ubiquitin- and SUMO-conjugated proteins in replicating chromatin domains leads to a reduction
377 in replication fork progression (30). We find that SUMOylation is broadly increased in
378 chromatin in *Rnf4*$^{\Delta/\Delta}$ cells (Supplemental Figure 4D) and this increase correlates with reduced
379 replication fork velocity and cell survival. In particular, we identified five out of eight
380 components of the mammalian SMC5/6 complex as hyper-SUMOylated chromatin constituents
381 in *Rnf4*$^{\Delta/\Delta}$ cells (Figure 4E and F). The SMC5/6 complex, like other SMC complexes, is a multi-
382 protein assembly that encircles DNA and facilitates loop extrusion (70). The SMC5/6 complex
383 facilitates DNA replication by helping to relieve chromosome-wide superhelical tension that
384 arises around active replisomes (71). This process involves the prevention of intertwining of
385 sister chromatid molecules behind the replication fork. Depletion of SMC5/6 in yeast causes a
386 block in replication at the ribosomal DNA array (39). The SMC5/6 complex furthermore
387 physically interacts with FANCI and FANCD2 in mammalian cells (72), therefore defects in the
388 regulation of SMC5/6 may account for the reduced accumulation of FANCI and FANCD2 at

389 replication forks in *Rnf4*$^{\Delta/\Delta}$ cells. The processivity of replication forks in budding yeast is
390 dependent on the SMC5/6 complex, which limits MPH1-mediated fork regression, and promotes
391 error-free bypass of DNA lesions (73, 74). The ability of SMC5 to promote lesion bypass is
392 dependent on SUMOylation, therefore it is an attractive candidate for regulation by RNF4.
393
394 Toxic recombination intermediates accumulate in cells with deficiencies in the SMC5/6 complex
395 (39, 40, 75). The cytotoxic effects of RNF4 deletion are notably rescued by RAD51 inhibitors,
396 indicating that RAD51-dependent recombination or fork regression is causative of cell death in
397 the absence of RNF4. It is possible that toxic RAD51-depenent structures arise because of a
398 failure to adequately regulate or localize the SMC5/6 complex in RNF4-deficient cells.
399 Mutations in *slx5*, the yeast homolog of RNF4, are known to produce gross chromosomal
400 rearrangements caused by aberrant recombination between homeologous sequences (76).
401 Although the importance and details of specific mechanisms for RNF4-dependent regulation of
402 DNA replication remain to be resolved, it is clear that RNF4 is required for efficient replication,
403 and may therefore represent an attractive target for cancer cases driven by *myc,* or other
404 oncogenes that drive rapid cellular proliferation.
405

406 Methods

407

408 *Sex as a biological variable*

409

410 Sex was not considered as a biological variable in this study.

411

412 *Generation of Rnf4 conditional knockout mice*

413

414 Cas9:sgRNA ribonucleoprotein complexes were prepared by incubating eSpCas9 (Millipore-
415 Sigma) with sgRNA and then adding single-stranded oligodeoxynucleotides, which contained
416 homology arms flanking LoxP sequences. This mixture was microinjected into C57BL/6J
417 embryos. The 5' LoxP sgRNA spacer sequence was CAATCACTTGCCTTATAAGA
418 (Millipore-Sigma) and the 5' LoxP oligo donor sequence was 5'-
419 CAAGATCTTAGGCAGGAAGATGGATGCCTTTGGTCAGACATGTTGGTTTTACTGAAA
420 ATCTCTGCCATTGTACCATGGGCTGAGCCTTCT**ATAACTTCGTATAGCATACATTA**
421 **TACGAAGTTAT**TATAAGGCAAGTGATTGGCCTCAGTGCCTGGACAGGACCTTCTGA
422 G-3' (LoxP in bold). For the 3' LoxP, the sgRNA spacer sequence was
423 TTGGGTTCAGCTGTCTGCTC and the 3' LoxP donor oligo sequence was 5'-
424 ACAAGTATCTTCCAAGCAGCTAGGTAGGCATATTTGGAATACAGGGTTGGGTTCAGC
425 TGTCTGa**ATAACTTCGTATAGCATACATTATACGAAGTTAT**CTCAGGATAGACCAA
426 TTGACAGACAGACAGGGCCATACATACTGACCAGGGTGTGCTTTTCGCT-3' (LoxP in
427 bold, sequence in lower case added to create XmnI restriction site for screening). Three founders

were determined to have both LoxP sites correctly inserted flanking *Rnf4* exon 6. A single line used for the study was backcrossed four times to C56Bl/6.

Cell culture

Primary B cells were isolated from mouse spleen and activated for in vitro culture with lipopolysaccharide and interleukin 4 as previously described (77). U2OS Dox-inducible Myc-GFP (U2OS-iMyc) cells (48) were seeded in triplicate with or without 0.5 μg/ml doxycycline treatment in a 24-well plate after siRNA transfection. Eight days after seeding, proliferation was assayed using CellTiter-Glo® Luminescent Cell Viability assay (#G7572, Promega) according to the manufacturer's instructions. PLAT-GP cells (Cell Biolabs) were cultured in DMEM containing 10% fetal bovine serum and 0.5% Penicillin-Streptomycin. For the in vivo SUMOylation assay, FLAG-Rad51 plasmid was transfected into siRNA-treated U2OS cells using Lipofectamine 2000. Cells were processed 24 hr after transfection as described (78).

Antibodies, chemicals and plasmids

Custom anti-RNF4 antibody was generated as previously described (79). Commercial antibodies used in this study include: SUMO2/3 (ab3742; Abcam), p53 (2524; CST), Cleaved caspase-3 (9661; CST), Tubulin (T8238, Sigma), KAP1-pS824 (A300-767A; Bethyl), CHK1-pS345 (2341; CST), CHK1 (sc-8408; Santa Cruz), γ-H2AX (05-636; Millipore), γ-H2AX-Alexa 488 (20304S; CST), Histone H3 (ab1791; Abcam), TOP2a (sc-365916; Santa Cruz), TOP2b (MAB6348; Novus), PARP1 (9542; CST), RNF10 (16936-1-AP; Proteintech). Antibody specific for mouse

POLD4 was provided by Marietta Lee. The following chemicals were used: olaparib (S1060; Selleckchem), hydroxyurea (H8627; Sigma Aldrich), aphidicolin (A4487; Sigma Aldrich), cisplatin (S1166; Selleckchem), MMS (129925; Sigma Aldrich), gemcitabine (G6423; Sigma Aldrich), P22077 (662142; Sigma Aldrich), P5091 (2277; Biovision), 2-D08 (SML1052; Sigma Aldrich), ML-792 (407886, MedKoo), RI-1 (SML1294; Sigma Aldrich), B-02 (SML0364; Sigma Aldrich). For plasmids, human *RAD51* cDNA was inserted into pRK5-FLAG and human *RNF4* cDNA was inserted into pMX-PIE-IRES-eGFP. Amino acid substitutions for *RNF4*-CS and *RNF4*-ΔSIM were performed as described (78, 80).

Chromatin fractionation and immunoprecipitation

For chromatin fractionation, harvested cells were gently resuspended in Buffer A (10 mM HEPES [pH7.9], 1.5 mM $MgCl_2$, 10 mM KCl, 0.05% NP-40, 0.5 mM DTT, 10 mM NEM, 50 mM glycerol-2-phosphate, supplemented with protease-inhibitor cocktail, Roche) and incubated for 10min on ice. Cell nuclei were collected by centrifugation (5 min, 1,300 x g, 4°C) and incubated in Buffer B (3 mM EDTA, 0.2 mM EGTA, 0.5 mM DTT, 10 mM NEM, 50mM glycerol-2-phosphate, and protease-inhibitor cocktail) for 30min. The chromatin component was collected by centrifugation (4 min, 1,700 x g, 4°C) and lysed with Buffer C (20mM HEPES [pH7.9], 500 mM NaCl, 1.5 mM $MgCl_2$, 0.2mM EDTA, 0.5 mM DTT, 125 U / ml benzonase, 10 mM NEM, 50 mM glycerol-2-phosphate, and protease-inhibitor cocktail). Lysates were incubated for 5 min at 37°C on a shaking heat block followed by 20 min incubation on ice. After centrifugation at 16,000 g for 20 min, supernatant containing chromatin-bound protein was collected. Anti-SUMO2/3 immunoprecipitation of chromatin fractions was performed after 10-

fold dilution of chromatin samples in dilution buffer (50 mM Tris-HCl [pH 7.5], 150 mM NaCl, 0.5% NP-40, 10 mM NEM, 50mM glycerol-2-phosphate, and protease-inhibitor cocktail), with protein G-Agarose used for collection.

Double-strand break repair reporter assay

The EJ-DR assay was performed as previously described (81). To induce incorporated I-Sce1, Shield1 (632189; Clontech) and triamcinolone (T6510; Sigma Aldrich) ligands were added to the media for 24 h. Where necessary, RAD51 inhibitors were added together with the Shield1 and triamcinolone. NHEJ and HR repair activity was assessed by quantification of DsRed- and GFP-positive cells on BD FACS Calibur system and analyzed on FlowJo (Tree Star) 48hrs after induction.

siRNA depletion

Cells were transfected with siRNA using Lipofectamine RNAiMAX (13778; Invitrogen). The following siRNA oligonucleotides were used in this study: MISSION siRNA Universal Negative Control #1 (SIC001, Sigma-Aldrich), siGENOME Human RNF4 siRNA set of 4 (M-006557-03; Dharmacon), siRNF4-1 (D-006557-03), siRNF4-2 (D-006557-04), siRNF4-3 (D-006557-05), siRNF-UTR (GGGCAUGAAAGGUUGAGAA), siGENOME Human BRCA1 siRNA set of 4 (M-003461-02; Dharmacon), siGENOME Human BRCA2 siRNA set of 4 (M-003462-01; Dharmacon).

Flow cytometry

For the CFSE proliferation assay, purified B cells were resuspended at 1x 10^7 cells/ml in RPMI medium, labeled with 5 μM CFSE for 10 min at 37°C, then cultured in RPMI medium with or without IL-4 and LPS for 72 h. The CFSE fluorescence of unstimulated cells was taken as 100% and the number of additional cell divisions was calculated according to reduced CFSE fluorescence as the cells divided. Number of cell divisions was calculated as $\log_2$(median intensity of unstimulated cells / median intensity of indicated cells). For EdU incorporation, B cells were pulsed with 30 μM EdU for 30 min, and fixed with ice-cold methanol for 20 min. EdU was detected using the Click-iT EdU Alexa Fluor-647 imaging kit. Cells were stained with DAPI to measure DNA content. For flow cytometry analysis of splenocyte populations, mouse splenocytes were treated with ACK lysis buffer for 5 min, then blocked with anti-CD16/CD32 antibody for 10 min at room temperature and labeled with B220-A647 (557683; BD) and CD43-PE (12-0431-82; Invitrogen) for 1 hr at 4°C. Cytometry was performed using a BD FACSCalibur or Cytek Aurora with analysis in FlowJo.

Alkaline Comet assay

Alkaline comet assays were performed using CometAssay kit (Trevigen) according to the manufacturer's protocol. Splenic B cells were cultured for 48 hrs in vitro and then treated with mock or 100 μM MMS treatment for 3 hrs. Images were acquired by Nikon Eclipse E800 epifluorescence microscope and analyzed with OpenComet software.

DNA combing and DNA fiber analysis

To measure fork speed, cells were incubated with 20 μM 5-chlorodeoxyuridine (CldU; C6891; Sigma-Aldrich) for 20 min, followed by 20 min of incubation with 100 μM 5-iododeoxyuridine (IdU; I7125; Sigma-Aldrich). Genomic DNA purification and combing on glass coverslips was performed using materials and a protocol from Genomic Vision. DNA fiber analysis was performed as described (82). The DNA was stained with anti-CldU antibody (ab6326; Abcam) and anti-IdU antibody (347580; BD) for 1 h, followed by incubation with secondary antibodies for 45 min. Images were acquired by Nikon Eclipse E800 epifluorescence microscope using a 40x objective and analyzed with ImageJ software.

iPOND

iPOND was performed as previously described (35).

Retroviral transduction

To express the human *RNF4* gene in B cells, retroviral vectors were transfected into PLAT-GP cells using Lipofectamine 2000. B cells were cultured for 36 hrs of in vitro culture and spinoculated with retroviral supernatants at 1150 g for 1.5 hr in the presence of 10 μg/ml polybrene. After 4 hr at 37°C, supernatants were replaced with normal medium. The percentage of GFP^+ and $DAPI^-$ B cells was measured with flow cytometry on Day 2 and Day 3 to check the infection rates and viability.

543

544 *Preparation of metaphase spreads and FISH*

545

546 Telomere DNA FISH analysis was performed and analyzed as previously described (77). Images
547 were acquired by an AxioImager.Z2 microscope (Zeiss) using a 60x objective with MetaSystems
548 automatic stage. At least 50 metaphases were analyzed for each experiment.

549

550 *Mass spectrometry*

551

552 Thirty micrograms of each sample were digested in-gel with trypsin (1:50 ratio, sequencing
553 grade, Thermo Scientific Cat#90058) and peptides extracted as described previously (83, 84).
554 Peptides were labeled with Thermo TMTpro 16 Plex (Lot #: WC320807) and prefractionated by
555 high-pH RPLC. Mass spectrometry was conducted using SPS-MS3 to measure reporter ion
556 intensities on an Orbitrap Eclipse Tribrid Mass Spectrometer (Thermo Fisher). Instrument
557 settings were for MS1: Orbitrap resolution 120,000, scan range from 350–1600 Th, automatic
558 gain control (AGC) target 1E6, maximum injection time 100 ms; for MS2, Top 5 (3 sec) duty
559 cycle, quadrupole ion trap, AGC 2E4, collision energy 35, maximum injection time 35 ms,
560 isolation window was set at 0.7; and for MS3, 10 MS2 fragment ions captured as MS3 precursors
561 using isolation waveforms with multiple frequency notches, Orbitrap AGC 1.5E5, maximum
562 injection time 54 ms in the higher-energy collisional dissociation (HCD) cell and fragmented
563 with HCD with collision energy of 55% and scanned in the Orbitrap with scan range 100-500
564 m/z. Peak lists were generated by Thermo Proteome Discoverer (v. 2.1) as MASCOT Generic
565 Format (MGF) files and combined MS2-MS3 peak lists searched against the Uniprot mouse

566 database using an in-house version of X!Tandem (GPM Fury) (85). TMT MS3 reporter ion
567 intensities were extracted with correction for isotope channel crossover using custom in-house
568 software and exported to Excel. For each protein, the sum of TMT MS3 intensities for all
569 corresponding peptides were first normalized to the sum of the TMT intensities for each channel
570 to account for differences in labeling efficiency or amount of protein labeled for each channel.
571 The mean of the four replicates for each genotype/time-point was used to generate ratios for
572 selected comparisons. Proteins were filtered for those with 2 or more assigned spectra. Proteins
573 showing an increase of >10% in *Rnf4*$^{\Delta/\Delta}$ cells relative to WT cells with a P value < 0.05 (t-test)
574 were considered for further analysis.
575
576 For data-independent acquisition, instrument settings were: MS scan range set to 400-1200 m/z,
577 with resolution 12,000, AGC 3E6 and ion time set as auto. Eight m/z windows were used to
578 sequentially isolate (AGC 4E5 and ion time auto) and fragment ions in the C-trap using a relative
579 collision energy of 30. MS/MS spectra were recorded with a resolution of 30,000. Data were
580 analyzed using DIA-NN 1.8.1 (86) with default settings for FASTA digest for library-free search
581 / library generation and deep learning-based spectra and retention time prediction using Uniprot
582 reference proteomes UP000000589 (mouse). Data were normalized using the MaxLFQ
583 algorithm (87) and total normalized precursor intensities for each protein group were filtered for
584 both PEP (an estimate of the posterior error probability for the precursor identification, based on
585 scoring with neural networks) filter <0.01 and PG.Q (Protein Group Q Value) filter <0.01. T-
586 tests were calculated as above.
587
588 *Statistics*

589

590 Statistical tests were performed as described. $P < 0.05$ was considered to be statistically
591 significant. Where shown, n.s. indicates not significant. * indicates a P value < 0.05. ** indicates
592 a P value < 0.01. *** indicates a P value < 0.001. **** indicates a P value < 0.0001. Data points
593 on graphs represent results from a minimum of n=3 biological replicates. For beeswarm plots,
594 small data points represent individual values from n=3 experiments, separately colored, and large
595 data points indicate the mean of each experiment.

596

597 *Analysis of genomic data sets*

598

599 Functional categorization and measurements of statistical over-representation of protein classes
600 was performed using PANTHER (panther.db). STRING analysis was performed using tools at
601 https://string-db.org. cBioPortal (https://www.cbioportal.org) was used to access data on 72
602 pediatric acute lymphoblastic leukemia patients studied as part of the Therapeutically Applicable
603 Research to Generate Effective Treatments initiative, phs000218 (TARGET Phase II). The data
604 used for this analysis are available at https://portal.gdc.cancer.gov/projects. Overall survival of
605 patients with tumors with high *RNF4* mRNA expression (RNASeq z-score vs RSEM ≥ 2.0) was
606 compared to patients with *RNF4* mRNA in the unaltered range. cBioPortal was additionally used
607 to retrieve data on survival of patients with above-median and below median *RNF4* expression in
608 tumor biopsies, based on samples from 1,082 breast adenocarcinoma patients and 501 lung
609 adenocarcinoma patients studied as part of the TCGA PanCancer Atlas project (88). Analysis of
610 RNF4 expression in multiple tumor types was based on TCGA data accessed with the University
611 of Alabama Cancer Data analysis portal (89)

612

613 *Study Approval*

614

615 Vertebrate animal studies were carried out under an animal protocol approved by the Rutgers

616 University Institutional Animal Care and Use Committee.

617

618 *Data availability*

619

620 Proteomic data sets were deposited to the MassIVE database with accession numbers

621 MSV000090142, MSV000093660 and MSV000093661. All data used for figures is available in

622 a Supporting Data Values file.

623

624

Author Contributions

Experiments were conceived by J.H. and S.F.B. and performed by JH, except mass spectrometry, which was performed by H.Z. The paper was written by S.F.B.

Acknowledgements

Work in the Bunting lab is funded by NCI P01CA250957. JH was supported by a NJCCR postdoctoral fellowship. This study involved support from the Rutgers Cancer Institute of New Jersey Genome Editing Shared Resource, P30CA072720-5922, and Histopathology Shared Resource, P30CA072720-5919. Mass spectrometry was supported by NIH grant S10OD025140 to Dr. Peter Lobel. Thanks to Dr. Steven Brill for assistance with generating anti-RNF4 antibody, Dr. Xiaolu Yang (U. Penn) for providing *Rnf4*$^{+/-}$ mice; Dr. David Levens (NCI CCR) for providing U2OS-iMYC cells; and Dr. Marietta Lee (NY Medical College) for providing anti-POLD4 antibody.

641 References

642

643 1. Rape M. Ubiquitylation at the crossroads of development and disease. *Nat Rev Mol Cell*
644 *Biol.* 2018;19(1):59-70.
645 2. Vertegaal ACO. Signalling mechanisms and cellular functions of SUMO. *Nat Rev Mol*
646 *Cell Biol.* 2022.
647 3. Garcia-Rodriguez N, Wong RP, and Ulrich HD. Functions of Ubiquitin and SUMO in
648 DNA Replication and Replication Stress. *Front Genet.* 2016;7:87.
649 4. Jackson SP, and Durocher D. Regulation of DNA damage responses by ubiquitin and
650 SUMO. *Mol Cell.* 2013;49(5):795-807.
651 5. DiBello A, Datta AB, Zhang X, and Wolberger C. Role of E2-RING Interactions in
652 Governing RNF4-Mediated Substrate Ubiquitination. *J Mol Biol.* 2016;428(23):4639-50.
653 6. Tatham MH, Geoffroy MC, Shen L, Plechanovova A, Hattersley N, Jaffray EG, et al.
654 RNF4 is a poly-SUMO-specific E3 ubiquitin ligase required for arsenic-induced PML
655 degradation. *Nat Cell Biol.* 2008;10(5):538-46.
656 7. Osman AEG, Anderson J, Churpek JE, Christ TN, Curran E, Godley LA, et al. Treatment
657 of Acute Promyelocytic Leukemia in Adults. *J Oncol Pract.* 2018;14(11):649-57.
658 8. Guzzo CM, Berndsen CE, Zhu J, Gupta V, Datta A, Greenberg RA, et al. RNF4-
659 dependent hybrid SUMO-ubiquitin chains are signals for RAP80 and thereby mediate the
660 recruitment of BRCA1 to sites of DNA damage. *Sci Signal.* 2012;5(253):ra88.
661 9. Hirota K, Tsuda M, Murai J, Takagi T, Keka IS, Narita T, et al. SUMO-targeted ubiquitin
662 ligase RNF4 plays a critical role in preventing chromosome loss. *Genes Cells.*
663 2014;19(10):743-54.
664 10. Luo K, Deng M, Li Y, Wu C, Xu Z, Yuan J, and Lou Z. CDK-mediated RNF4
665 phosphorylation regulates homologous recombination in S-phase. *Nucleic Acids Res.*
666 2015;43(11):5465-75.
667 11. Luo K, Zhang H, Wang L, Yuan J, and Lou Z. Sumoylation of MDC1 is important for
668 proper DNA damage response. *EMBO J.* 2012;31(13):3008-19.
669 12. Xie J, Kim H, Moreau LA, Puhalla S, Garber J, Al Abo M, et al. RNF4-mediated
670 polyubiquitination regulates the Fanconi anemia/BRCA pathway. *J Clin Invest.*
671 2015;125(4):1523-32.
672 13. Galanty Y, Belotserkovskaya R, Coates J, and Jackson SP. RNF4, a SUMO-targeted
673 ubiquitin E3 ligase, promotes DNA double-strand break repair. *Genes Dev.*
674 2012;26(11):1179-95.
675 14. Yin Y, Seifert A, Chua JS, Maure JF, Golebiowski F, and Hay RT. SUMO-targeted
676 ubiquitin E3 ligase RNF4 is required for the response of human cells to DNA damage.
677 *Genes Dev.* 2012;26(11):1196-208.
678 15. Liu JCY, Kuhbacher U, Larsen NB, Borgermann N, Garvanska DH, Hendriks IA, et al.
679 Mechanism and function of DNA replication-independent DNA-protein crosslink repair
680 via the SUMO-RNF4 pathway. *EMBO J.* 2021;40(18):e107413.
681 16. Helleday T. Homologous recombination in cancer development, treatment and
682 development of drug resistance. *Carcinogenesis.* 2010;31(6):955-60.
683 17. Nguyen L, J WMM, Van Hoeck A, and Cuppen E. Pan-cancer landscape of homologous
684 recombination deficiency. *Nat Commun.* 2020;11(1):5584.

18. O'Kane GM, Connor AA, and Gallinger S. Characterization, Detection, and Treatment Approaches for Homologous Recombination Deficiency in Cancer. *Trends Mol Med.* 2017;23(12):1121-37.
19. Hu XV, Rodrigues TM, Tao H, Baker RK, Miraglia L, Orth AP, et al. Identification of RING finger protein 4 (RNF4) as a modulator of DNA demethylation through a functional genomics screen. *Proc Natl Acad Sci U S A.* 2010;107(34):15087-92.
20. Cao L, Xu X, Bunting SF, Liu J, Wang RH, Cao LL, et al. A selective requirement for 53BP1 in the biological response to genomic instability induced by Brca1 deficiency. *Mol Cell.* 2009;35(4):534-41.
21. Rickert RC, Roes J, and Rajewsky K. B lymphocyte-specific, Cre-mediated mutagenesis in mice. *Nucleic Acids Res.* 1997;25(6):1317-8.
22. Marechal A, and Zou L. DNA damage sensing by the ATM and ATR kinases. *Cold Spring Harb Perspect Biol.* 2013;5(9).
23. Xu X, Wagner KU, Larson D, Weaver Z, Li C, Ried T, et al. Conditional mutation of Brca1 in mammary epithelial cells results in blunted ductal morphogenesis and tumour formation. *Nat Genet.* 1999;22(1):37-43.
24. Groth P, Auslander S, Majumder MM, Schultz N, Johansson F, Petermann E, and Helleday T. Methylated DNA causes a physical block to replication forks independently of damage signalling, O(6)-methylguanine or DNA single-strand breaks and results in DNA damage. *J Mol Biol.* 2010;402(1):70-82.
25. Hashimoto Y, Ray Chaudhuri A, Lopes M, and Costanzo V. Rad51 protects nascent DNA from Mre11-dependent degradation and promotes continuous DNA synthesis. *Nat Struct Mol Biol.* 2010;17(11):1305-11.
26. Soll JM, Sobol RW, and Mosammaparast N. Regulation of DNA Alkylation Damage Repair: Lessons and Therapeutic Opportunities. *Trends Biochem Sci.* 2017;42(3):206-18.
27. Harrigan JA, Belotserkovskaya R, Coates J, Dimitrova DS, Polo SE, Bradshaw CR, et al. Replication stress induces 53BP1-containing OPT domains in G1 cells. *J Cell Biol.* 2011;193(1):97-108.
28. Lukas C, Savic V, Bekker-Jensen S, Doil C, Neumann B, Pedersen RS, et al. 53BP1 nuclear bodies form around DNA lesions generated by mitotic transmission of chromosomes under replication stress. *Nat Cell Biol.* 2011;13(3):243-53.
29. Yazinski SA, and Zou L. Functions, Regulation, and Therapeutic Implications of the ATR Checkpoint Pathway. *Annu Rev Genet.* 2016;50:155-73.
30. Lecona E, Rodriguez-Acebes S, Specks J, Lopez-Contreras AJ, Ruppen I, Murga M, et al. USP7 is a SUMO deubiquitinase essential for DNA replication. *Nat Struct Mol Biol.* 2016;23(4):270-7.
31. Kim YS, Keyser SG, and Schneekloth JS, Jr. Synthesis of 2',3',4'-trihydroxyflavone (2-D08), an inhibitor of protein sumoylation. *Bioorg Med Chem Lett.* 2014;24(4):1094-7.
32. He X, Riceberg J, Soucy T, Koenig E, Minissale J, Gallery M, et al. Probing the roles of SUMOylation in cancer cell biology by using a selective SAE inhibitor. *Nat Chem Biol.* 2017;13(11):1164-71.
33. Ding L, Luo Y, Tian T, Chen X, Yang Y, Bu M, et al. RNF4 controls the extent of replication fork reversal to preserve genome stability. *Nucleic Acids Res.* 2022;50(10):5672-87.

34. Kumar R, Gonzalez-Prieto R, Xiao Z, Verlaan-de Vries M, and Vertegaal ACO. The STUbL RNF4 regulates protein group SUMOylation by targeting the SUMO conjugation machinery. *Nat Commun.* 2017;8(1):1809.
35. Sirbu BM, McDonald WH, Dungrawala H, Badu-Nkansah A, Kavanaugh GM, Chen Y, et al. Identification of proteins at active, stalled, and collapsed replication forks using isolation of proteins on nascent DNA (iPOND) coupled with mass spectrometry. *J Biol Chem.* 2013;288(44):31458-67.
36. Niraj J, Farkkila A, and D'Andrea AD. The Fanconi Anemia Pathway in Cancer. *Annu Rev Cancer Biol.* 2019;3:457-78.
37. Byrd AK, and Raney KD. Structure and function of Pif1 helicase. *Biochem Soc Trans.* 2017;45(5):1159-71.
38. Urban V, Dobrovolna J, Huhn D, Fryzelkova J, Bartek J, and Janscak P. RECQ5 helicase promotes resolution of conflicts between replication and transcription in human cells. *J Cell Biol.* 2016;214(4):401-15.
39. Peng XP, and Zhao X. The multi-functional Smc5/6 complex in genome protection and disease. *Nat Struct Mol Biol.* 2023;30(6):724-34.
40. Menolfi D, Delamarre A, Lengronne A, Pasero P, and Branzei D. Essential Roles of the Smc5/6 Complex in Replication through Natural Pausing Sites and Endogenous DNA Damage Tolerance. *Mol Cell.* 2015;60(6):835-46.
41. Budke B, Logan HL, Kalin JH, Zelivianskaia AS, Cameron McGuire W, Miller LL, et al. RI-1: a chemical inhibitor of RAD51 that disrupts homologous recombination in human cells. *Nucleic Acids Res.* 2012;40(15):7347-57.
42. Huang F, and Mazin AV. A small molecule inhibitor of human RAD51 potentiates breast cancer cell killing by therapeutic agents in mouse xenografts. *PLoS One.* 2014;9(6):e100993.
43. Jonkers J, Meuwissen R, van der Gulden H, Peterse H, van der Valk M, and Berns A. Synergistic tumor suppressor activity of BRCA2 and p53 in a conditional mouse model for breast cancer. *Nat Genet.* 2001;29(4):418-25.
44. Liu X, Holstege H, van der Gulden H, Treur-Mulder M, Zevenhoven J, Velds A, et al. Somatic loss of BRCA1 and p53 in mice induces mammary tumors with features of human BRCA1-mutated basal-like breast cancer. *Proc Natl Acad Sci U S A.* 2007;104(29):12111-6.
45. Xu X, Qiao W, Linke SP, Cao L, Li WM, Furth PA, et al. Genetic interactions between tumor suppressors Brca1 and p53 in apoptosis, cell cycle and tumorigenesis. *Nat Genet.* 2001;28(3):266-71.
46. Donehower LA, Harvey M, Slagle BL, McArthur MJ, Montgomery CA, Jr., Butel JS, and Bradley A. Mice deficient for p53 are developmentally normal but susceptible to spontaneous tumours. *Nature.* 1992;356(6366):215-21.
47. Adams JM, Harris AW, Pinkert CA, Corcoran LM, Alexander WS, Cory S, et al. The c-myc oncogene driven by immunoglobulin enhancers induces lymphoid malignancy in transgenic mice. *Nature.* 1985;318(6046):533-8.
48. Nie Z, Guo C, Das SK, Chow CC, Batchelor E, Simons SSJ, and Levens D. Dissecting transcriptional amplification by MYC. *Elife.* 2020;9.
49. Matos-Rodrigues G, Guirouilh-Barbat J, Martini E, and Lopez BS. Homologous recombination, cancer and the 'RAD51 paradox'. *NAR Cancer.* 2021;3(2):zcab016.

50. Sonoda E, Sasaki MS, Buerstedde JM, Bezzubova O, Shinohara A, Ogawa H, et al. Rad51-deficient vertebrate cells accumulate chromosomal breaks prior to cell death. *EMBO J.* 1998;17(2):598-608.
51. Ameziane N, May P, Haitjema A, van de Vrugt HJ, van Rossum-Fikkert SE, Ristic D, et al. A novel Fanconi anaemia subtype associated with a dominant-negative mutation in RAD51. *Nat Commun.* 2015;6:8829.
52. Lim DS, and Hasty P. A mutation in mouse rad51 results in an early embryonic lethal that is suppressed by a mutation in p53. *Mol Cell Biol.* 1996;16(12):7133-43.
53. Tsuzuki T, Fujii Y, Sakumi K, Tominaga Y, Nakao K, Sekiguchi M, et al. Targeted disruption of the Rad51 gene leads to lethality in embryonic mice. *Proc Natl Acad Sci U S A.* 1996;93(13):6236-40.
54. Hoellein A, Fallahi M, Schoeffmann S, Steidle S, Schaub FX, Rudelius M, et al. Myc-induced SUMOylation is a therapeutic vulnerability for B-cell lymphoma. *Blood.* 2014;124(13):2081-90.
55. Luo J, Solimini NL, and Elledge SJ. Principles of cancer therapy: oncogene and non-oncogene addiction. *Cell.* 2009;136(5):823-37.
56. Gilad O, Nabet BY, Ragland RL, Schoppy DW, Smith KD, Durham AC, and Brown EJ. Combining ATR suppression with oncogenic Ras synergistically increases genomic instability, causing synthetic lethality or tumorigenesis in a dosage-dependent manner. *Cancer Res.* 2010;70(23):9693-702.
57. Murga M, Campaner S, Lopez-Contreras AJ, Toledo LI, Soria R, Montana MF, et al. Exploiting oncogene-induced replicative stress for the selective killing of Myc-driven tumors. *Nat Struct Mol Biol.* 2011;18(12):1331-5.
58. Ragland RL, Patel S, Rivard RS, Smith K, Peters AA, Bielinsky AK, and Brown EJ. RNF4 and PLK1 are required for replication fork collapse in ATR-deficient cells. *Genes Dev.* 2013;27(20):2259-73.
59. Ellis N, Zhu J, Yagle MK, Yang WC, Huang J, Kwako A, et al. RNF4 Regulates the BLM Helicase in Recovery From Replication Fork Collapse. *Front Genet.* 2021;12:753535.
60. Tian T, Bu M, Chen X, Ding L, Yang Y, Han J, et al. The ZATT-TOP2A-PICH Axis Drives Extensive Replication Fork Reversal to Promote Genome Stability. *Mol Cell.* 2021;81(1):198-211 e6.
61. Sciascia N, Wu W, Zong D, Sun Y, Wong N, John S, et al. Suppressing proteasome mediated processing of topoisomerase II DNA-protein complexes preserves genome integrity. *Elife.* 2020;9.
62. Sun Y, Miller Jenkins LM, Su YP, Nitiss KC, Nitiss JL, and Pommier Y. A conserved SUMO pathway repairs topoisomerase DNA-protein cross-links by engaging ubiquitin-mediated proteasomal degradation. *Sci Adv.* 2020;6(46).
63. Krastev DB, Li S, Sun Y, Wicks AJ, Hoslett G, Weekes D, et al. The ubiquitin-dependent ATPase p97 removes cytotoxic trapped PARP1 from chromatin. *Nat Cell Biol.* 2022;24(1):62-73.
64. Martin N, Schwamborn K, Schreiber V, Werner A, Guillier C, Zhang XD, et al. PARP-1 transcriptional activity is regulated by sumoylation upon heat shock. *EMBO J.* 2009;28(22):3534-48.
65. Murai J, Huang SY, Das BB, Renaud A, Zhang Y, Doroshow JH, et al. Trapping of PARP1 and PARP2 by Clinical PARP Inhibitors. *Cancer Res.* 2012;72(21):5588-99.

66. Schlacher K, Wu H, and Jasin M. A distinct replication fork protection pathway connects Fanconi anemia tumor suppressors to RAD51-BRCA1/2. *Cancer Cell.* 2012;22(1):106-16.
67. Schwab RA, Blackford AN, and Niedzwiedz W. ATR activation and replication fork restart are defective in FANCM-deficient cells. *EMBO J.* 2010;29(4):806-18.
68. Yang Y, Xu W, Gao F, Wen C, Zhao S, Yu Y, et al. Transcription-replication conflicts in primordial germ cells necessitate the Fanconi anemia pathway to safeguard genome stability. *Proc Natl Acad Sci U S A.* 2022;119(34):e2203208119.
69. Lecona E, and Fernandez-Capetillo O. A SUMO and ubiquitin code coordinates protein traffic at replication factories. *Bioessays.* 2016;38(12):1209-17.
70. Pradhan B, Kanno T, Umeda Igarashi M, Loke MS, Baaske MD, Wong JSK, et al. The Smc5/6 complex is a DNA loop-extruding motor. *Nature.* 2023;616(7958):843-8.
71. Kegel A, Betts-Lindroos H, Kanno T, Jeppsson K, Strom L, Katou Y, et al. Chromosome length influences replication-induced topological stress. *Nature.* 2011;471(7338):392-6.
72. Rossi F, Helbling-Leclerc A, Kawasumi R, Jegadesan NK, Xu X, Devulder P, et al. SMC5/6 acts jointly with Fanconi anemia factors to support DNA repair and genome stability. *EMBO Rep.* 2020;21(2):e48222.
73. Xue X, Choi K, Bonner JN, Chiba T, Kwon Y, Xu Y, et al. Restriction of replication fork regression activities by a conserved SMC complex. *Mol Cell.* 2014;56(3):436-45.
74. Zapatka M, Pocino-Merino I, Heluani-Gahete H, Bermudez-Lopez M, Tarres M, Ibars E, et al. Sumoylation of Smc5 Promotes Error-free Bypass at Damaged Replication Forks. *Cell Rep.* 2019;29(10):3160-72 e4.
75. Agashe S, Joseph CR, Reyes TAC, Menolfi D, Giannattasio M, Waizenegger A, et al. Smc5/6 functions with Sgs1-Top3-Rmi1 to complete chromosome replication at natural pause sites. *Nat Commun.* 2021;12(1):2111.
76. Albuquerque CP, Wang G, Lee NS, Kolodner RD, Putnam CD, and Zhou H. Distinct SUMO ligases cooperate with Esc2 and Slx5 to suppress duplication-mediated genome rearrangements. *PLoS Genet.* 2013;9(8):e1003670.
77. Misenko SM, and Bunting SF. Rapid analysis of chromosome aberrations in mouse B lymphocytes by PNA-FISH. *J Vis Exp.* 2014(90).
78. Her J, Jeong YY, and Chung IK. PIAS1-mediated sumoylation promotes STUbL-dependent proteasomal degradation of the human telomeric protein TRF2. *FEBS Lett.* 2015;589(21):3277-86.
79. Sharma P, Mullen JR, Li M, Zaratiegui M, Bunting SF, and Brill SJ. A Lysine Desert Protects a Novel Domain in the Slx5-Slx8 SUMO Targeted Ub Ligase To Maintain Sumoylation Levels in Saccharomyces cerevisiae. *Genetics.* 2017;206(4):1807-21.
80. Rojas-Fernandez A, Plechanovova A, Hattersley N, Jaffray E, Tatham MH, and Hay RT. SUMO chain-induced dimerization activates RNF4. *Mol Cell.* 2014;53(6):880-92.
81. Bindra RS, Goglia AG, Jasin M, and Powell SN. Development of an assay to measure mutagenic non-homologous end-joining repair activity in mammalian cells. *Nucleic Acids Res.* 2013;41(11):e115.
82. Her J, Ray C, Altshuler J, Zheng H, and Bunting SF. 53BP1 Mediates ATR-Chk1 Signaling and Protects Replication Forks under Conditions of Replication Stress. *Mol Cell Biol.* 2018;38(8).
83. Sleat DE, Della Valle MC, Zheng H, Moore DF, and Lobel P. The mannose 6-phosphate glycoprotein proteome. *J Proteome Res.* 2008;7(7):3010-21.

84. Sleat DE, Lackland H, Wang Y, Sohar I, Xiao G, Li H, and Lobel P. The human brain mannose 6-phosphate glycoproteome: a complex mixture composed of multiple isoforms of many soluble lysosomal proteins. *Proteomics.* 2005;5(6):1520-32.
85. Craig R, and Beavis RC. TANDEM: matching proteins with tandem mass spectra. *Bioinformatics.* 2004;20(9):1466-7.
86. Demichev V, Messner CB, Vernardis SI, Lilley KS, and Ralser M. DIA-NN: neural networks and interference correction enable deep proteome coverage in high throughput. *Nat Methods.* 2020;17(1):41-4.
87. Cox J, Hein MY, Luber CA, Paron I, Nagaraj N, and Mann M. Accurate proteome-wide label-free quantification by delayed normalization and maximal peptide ratio extraction, termed MaxLFQ. *Mol Cell Proteomics.* 2014;13(9):2513-26.
88. Hoadley KA, Yau C, Hinoue T, Wolf DM, Lazar AJ, Drill E, et al. Cell-of-Origin Patterns Dominate the Molecular Classification of 10,000 Tumors from 33 Types of Cancer. *Cell.* 2018;173(2):291-304 e6.
89. Chandrashekar DS, Bashel B, Balasubramanya SAH, Creighton CJ, Ponce-Rodriguez I, Chakravarthi B, and Varambally S. UALCAN: A Portal for Facilitating Tumor Subgroup Gene Expression and Survival Analyses. *Neoplasia.* 2017;19(8):649-58.

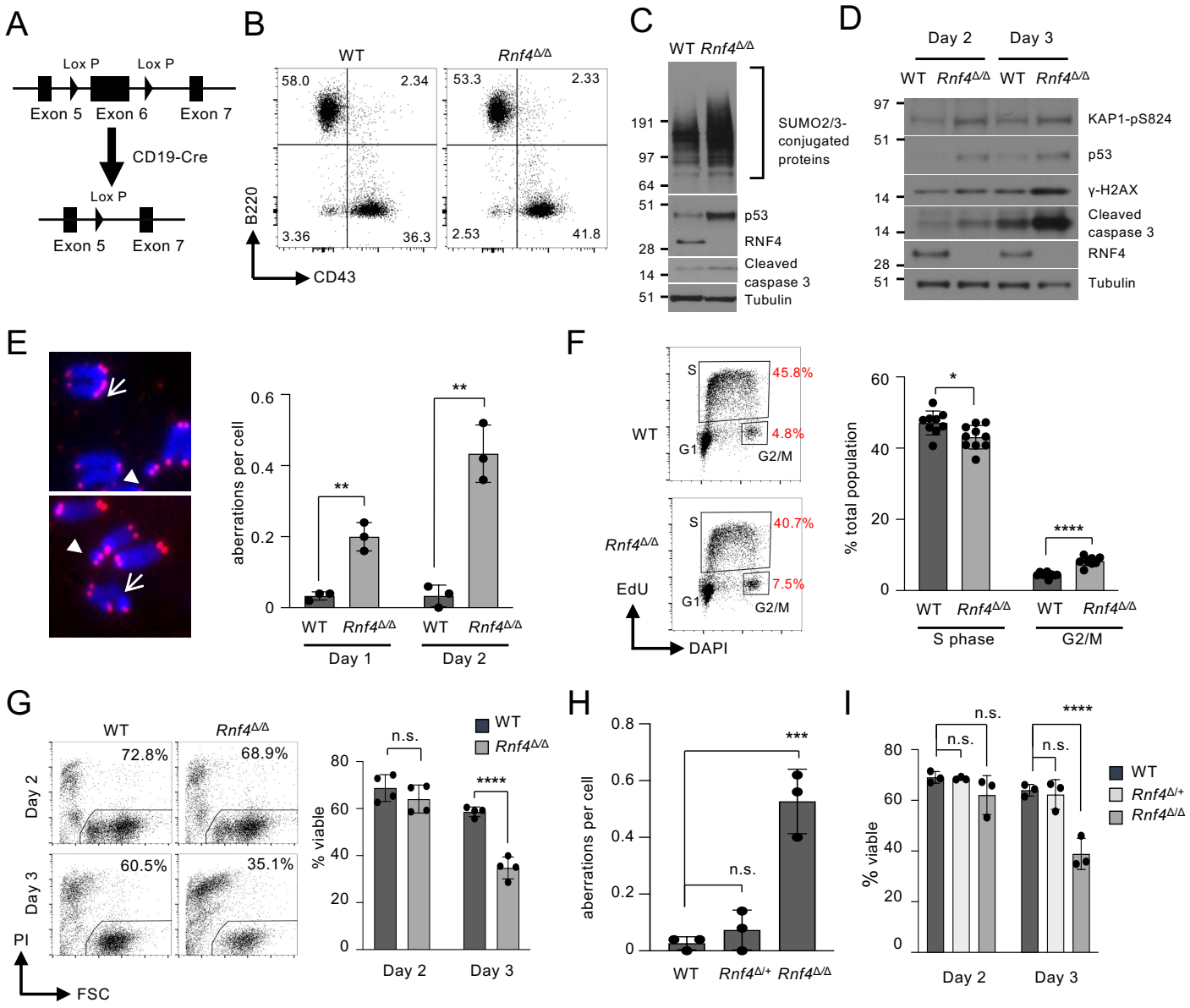

Figure 1. Genomic instability and apoptosis in RNF4 conditional-knockout B cells. (**A**) Schematic representation of Cre-induced deletion of *Rnf4* exon 6. (**B**) Flow cytometry analysis of cell populations in the spleens of WT and *Rnf4*-conditional-knockout ($Rnf4^{\Delta/\Delta}$) mice. (**C**) Western blot analysis of protein expression in $Rnf4^{\Delta/\Delta}$ B cells after 2 days activation in vitro. (**D**) Western blot to measure induction of markers of DNA damage signaling in activated WT and $Rnf4^{\Delta/\Delta}$ B cells after 2 days and 3 days of in vitro culture. (**E**) Analysis of chromosome aberrations in metaphase spreads prepared from WT and $Rnf4^{\Delta/\Delta}$ B cells after one or two days of in vitro culture. White arrows show examples of chromosome rearrangements and solid arrowheads show examples of chromosome breaks. (**F**) Cell cycle analysis of fixed B cells after 48 hrs activation in vitro. (**G**) Flow cytometry analysis of cell death in splenic B cells cultured for 2 or 3 days in vitro. Left, figures indicate the percentage of cells that remained viable, based on propidium iodide exclusion. (**H**) Chromosome aberrations in metaphase spreads from WT, $Rnf4^{\Delta/+}$, and $Rnf4^{\Delta/\Delta}$ B cells. (**I**) Viability of B cells after 2 and 3 days of in vitro culture, measured by DAPI exclusion. Error bars where shown indicate S.D. of the mean. P values were calculated with unpaired t-test (**E**, **F**, **G**), one-way ANOVA with Dunnett's multiple comparisons test (**H**), and two-way ANOVA with Dunnett's multiple comparisons test (**I**).

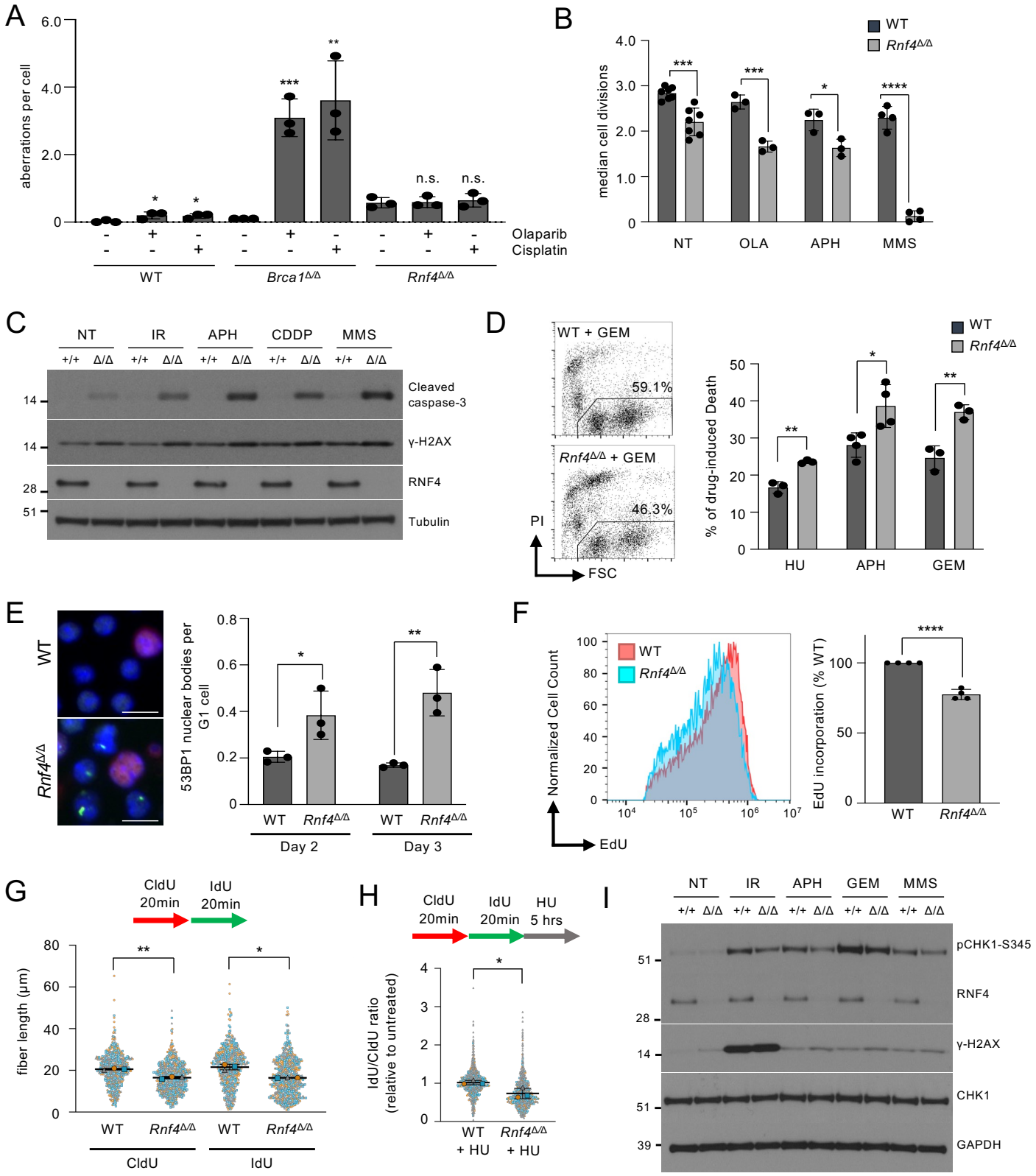

Figure 2. *Rnf4*$^{\Delta/\Delta}$ B cells show defects in DNA replication. (**A**) Analysis of chromosome aberrations in B lymphocytes treated overnight ± 2 μM olaparib or 1 μM cisplatin. Statistical differences between the means of the treated and non-treated samples are shown. (**B**) Flow cytometry analysis of CFSE dilution to measure B cell growth over 72 hrs. Chart shows quantification of cell doublings based on CFSE fluorescence. (**C**) Western blot analysis of caspase-3 cleavage and γ-H2AX after no treatment (NT), or after overnight recovery from treatment with 2 Gy of ionizing radiation (IR), 0.4 μM aphidicolin (APH), 2.5 μM cisplatin (CDDP), or 100 μM MMS. (**D**) Sample flow cytometry data quantifying cell viability after treatment with gemcitabine (GEM). Gated population shows the viable, PI-negative population. Graph shows proportion of cells that became non-viable 24 hrs post-treatment with either hydroxyurea (HU) (4 mM, 3 hrs), APH (40 μM, 2 hrs), or GEM (250 nM, 2 hrs). (**E**) Immunofluorescent detection of 53BP1 G1 nuclear bodies (green) in B cells after in vitro culture. Cyclin A staining (red) reveals S/G2-phase cells. (**F**) EdU uptake measured by flow cytometry. (**G**) Analysis of nascent DNA tract length in WT and *Rnf4*$^{\Delta/\Delta}$ splenic B cells by DNA combing. Mean ± S.D. of n=3 experiments shown. (**H**) Stability of nascent DNA measured by fiber analysis after 4mM HU treatment. Mean ± S.D. of n=3 experiments shown. (**I**) Western blot to show induction of pCHK1 in WT and *Rnf4*$^{\Delta/\Delta}$ cells after IR (30Gy, 2hrs recovery), APH (0.4 μM, overnight), GEM (100 nM, 2 hrs), MMS (200 μM, 3 hrs). Error bars in Parts **A**, **B**, **D**, **E**, and **F** show S.D. of the mean, with P values calculated by unpaired t-test. P values in Parts **G** and **H** calculated by paired t-test.

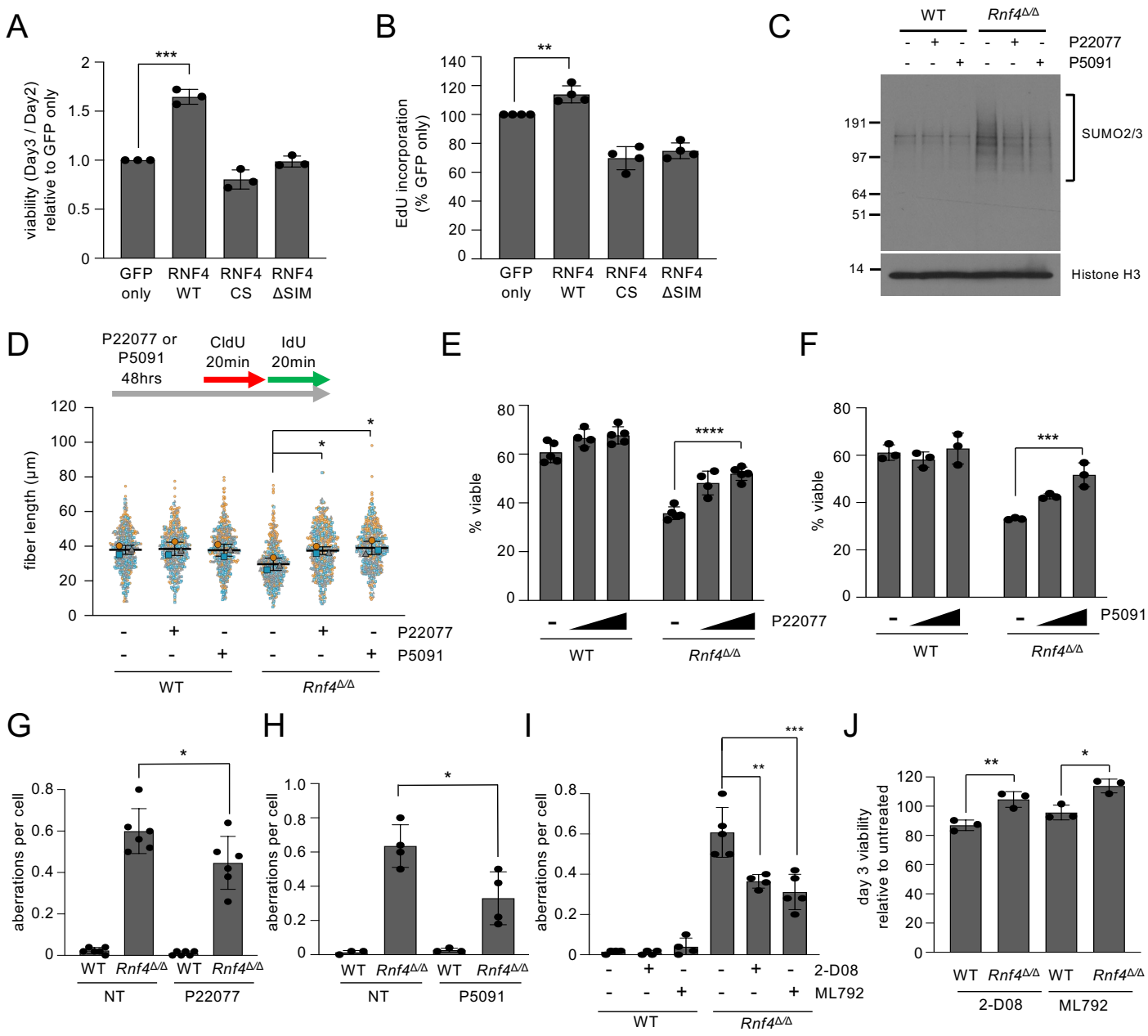

Figure 3. Phenotypes of *Rnf4*$^{\Delta/\Delta}$ cells are caused by accumulation of SUMOylated proteins (**A**) Analysis of viability of *Rnf4*$^{\Delta/\Delta}$ cells transduced with constructs expressing GFP, WT RNF4, a catalytic mutant of RNF4 (RNF4-CS) or RNF4 defective for SUMO binding (RNF4-ΔSIM). (**B**) Quantification of EdU uptake by *Rnf4*$^{\Delta/\Delta}$ cells transduced with GFP or RNF4 cDNAs. (**C**) Western blot of cells grown in vitro for two days ± continual treatment with USP7 inhibitors, P22077 (2 μM) or P5091 (1 μM). (**D**) Analysis of nascent DNA tract length in WT and *Rnf4*$^{\Delta/\Delta}$ B cells. Cells were cultured in vitro for 48 hrs ± P22077 (2 μM) or P5091 (1 μM), then incubated with CldU for 20 min, followed by IdU for 20 min. CldU and IdU tract lengths were analyzed after DNA combing. Mean ± S.D. of n=3 experiments shown. (**E**) Cell viability after 72 hrs culture ± P22077 (1 μM, 2 μM). Viable cells were identified based on ability to exclude DAPI. (**F**) As (**E**), using P5091 (0.5 μM, 1 μM). (**G**) Analysis of chromosome aberrations in B cells cultured 48 hrs ± P22077 treatment (2 μM). (**H**), as (**G**), using P5091 (1 μM). (**I**) Analysis of chromosome aberrations in B cells cultured 48 hrs ± continuous treatment with the SUMO inhibitors, 2-D08 (40 μM) or ML-792 (20 nM). (**J**) Cell viability measured by quantification of DAPI-negative cells after 72 hrs culture ± 2-D08 (40 μM) or ML-792 (20 nM). Error bars in parts **A**, **B**, and **E-J**, show S.D. of the mean. P values were calculated with unpaired t-test (**A**, **B**, **J**), one-way ANOVA with Dunnett's multiple comparison test, (**D**, **I**), two-way ANOVA with Dunnett's multiple comparison test (**E**, **F**), and one-way ANOVA with Tukey's multiple comparison test (**G**, **H**).

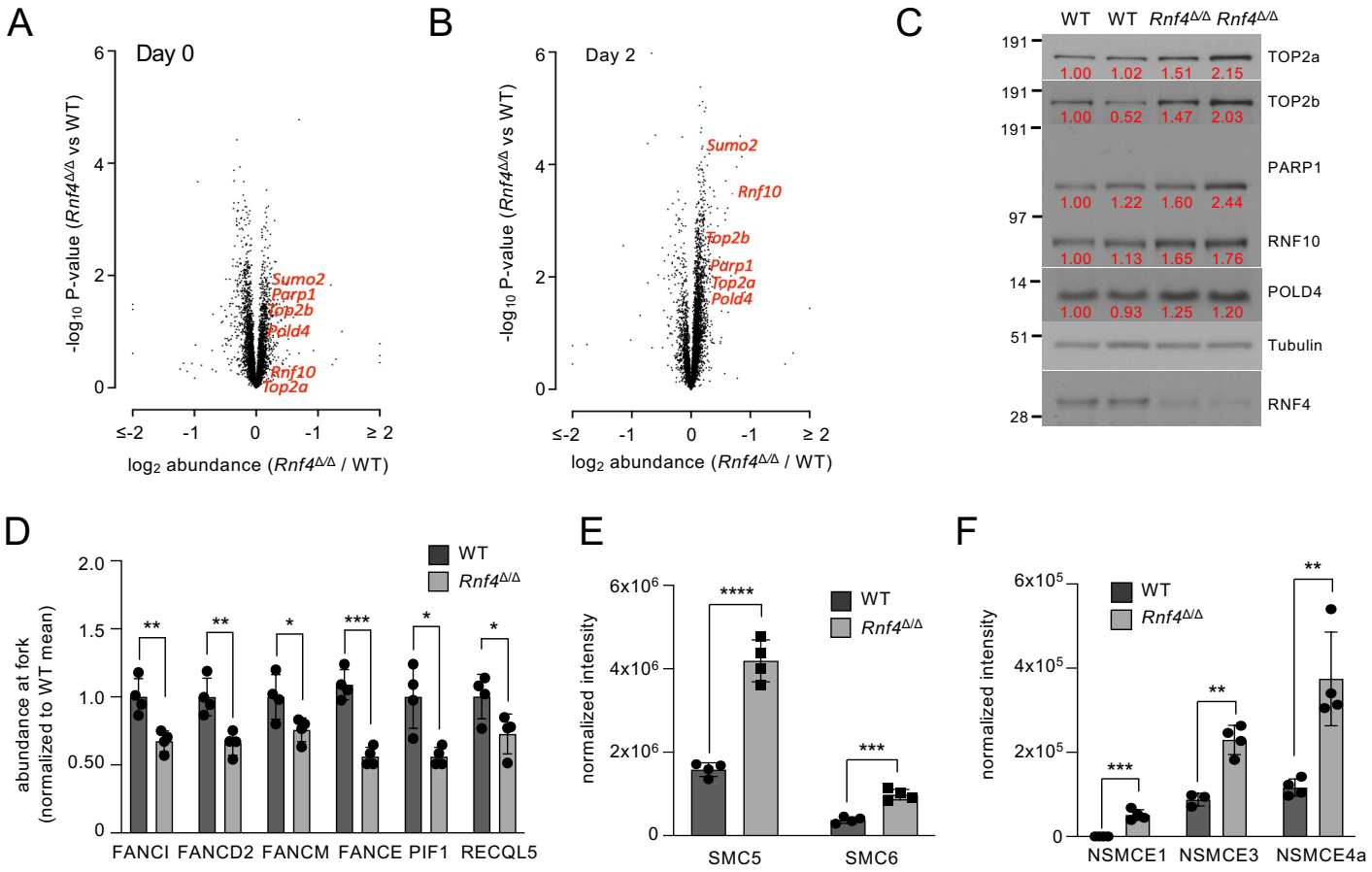

Figure 4: RNF4 deficiency leads to reduced accumulation of proteins needed for replication stress responses at replication forks. (**A**) Volcano plot showing protein abundance in resting *Rnf4*$^{\Delta/\Delta}$ B cells relative to WT controls. Each data point represents the average of four samples. Six proteins that showed increased abundance after B cell activation are labeled. (**B**) Volcano plot of B cells after 48 hrs in vitro culture with cell proliferation induced by addition of LPS. (**C**) Western blot showing expression of proteins in WT and *Rnf4*$^{\Delta/\Delta}$ B cells after 48 hrs culture. Two samples are shown in each case. Figures in red indicate band intensities measured with ImageJ. (**D**) Abundance of proteins required for replication stress responses at replication forks, measured by iPOND-MS, in WT and *Rnf4*$^{\Delta/\Delta}$ B cells. (**E**) Increase in abundance of SUMOylated SMC5 and SMC6 in *Rnf4*$^{\Delta/\Delta}$ cells, measured by mass spectrometry after SUMO2/3 immunoprecipitation of chromatin from WT and *Rnf4*$^{\Delta/\Delta}$ cells. (**F**) Increase in abundance of SUMOylated Non-SMC Element (NSMCE) subunits of the SMC5/6 complex in chromatin of *Rnf4*$^{\Delta/\Delta}$ cells. Error bars in parts **D**-**F** show S.D. of the mean of n=4 replicates. P values were calculated by unpaired t-test. P < 0.05 was considered significant.

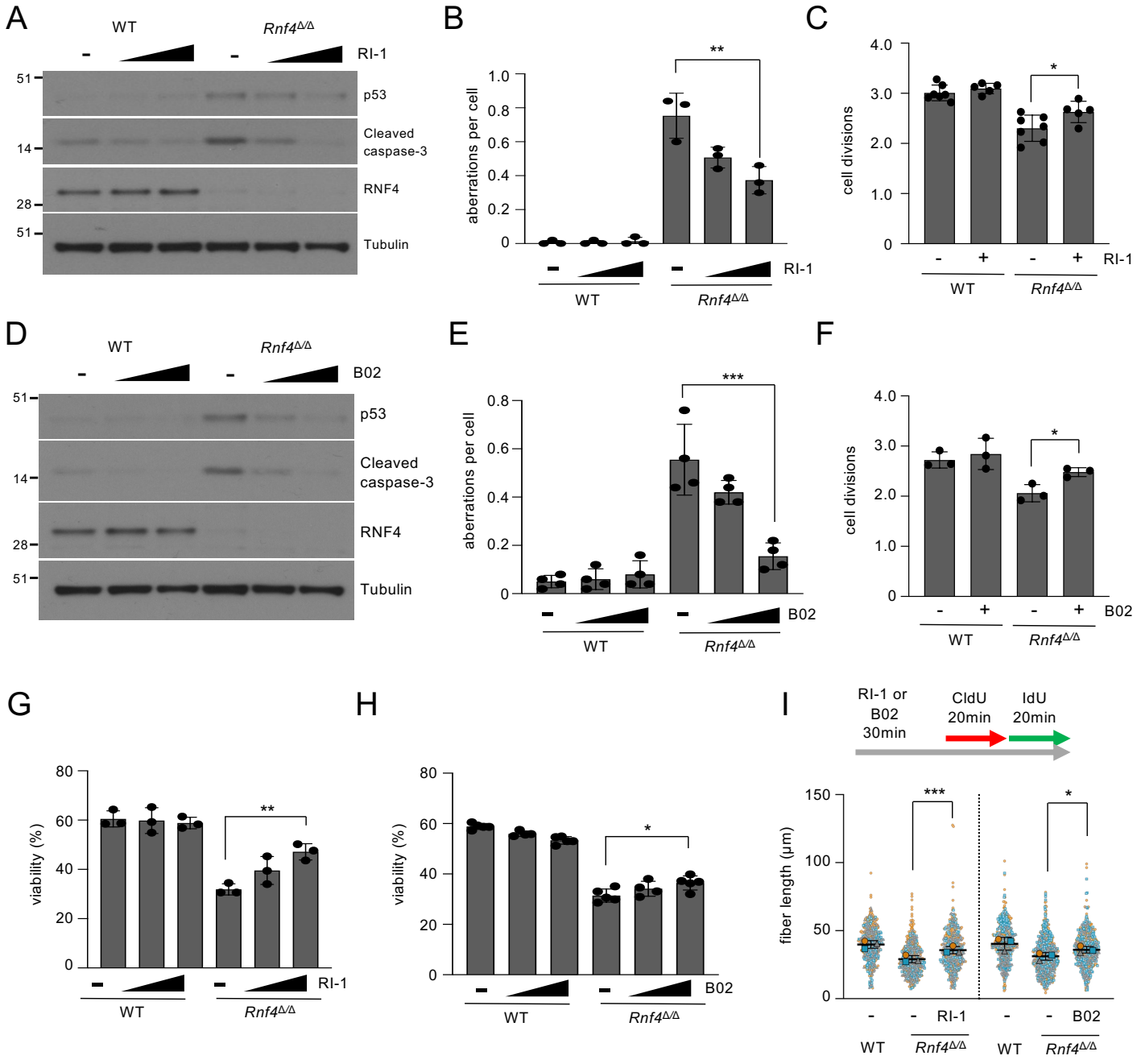

Figure 5: Genomic instability and cell death in RNF4-deficient cells is dependent on RAD51. (**A**) Western blot analysis of WT and *Rnf4*$^{\Delta/\Delta}$ B cells cultured in vitro for 72 hrs with mock treatment (-) or with the RAD51 inhibitor, RI-1 (5 μM, 10 μM). (**B**) Analysis of chromosome aberrations in Day 2 cultured B cells ± RI-1 treatment (5 μM, 10 μM). (**C**) Analysis of CFSE FACS to measure cell proliferation during 72 hrs growth ± RI-1 treatment (5 μM). (**D**) As (**A**) with the RAD51 inhibitor, B02 (5 μM, 10 μM). (**E**) As (**B**), with B02 (5 μM, 10 μM). (**F**) As (**C**) with B02 (5 μM). (**G**) Viability of B cells, measured by DAPI exclusion, after treatment with RI-1 (5 μM, 10 μM) on Day 3. (**H**) As (**G**) with B02 (2.5 μM, 5 μM). (**I**) Measurement of newly-replicated DNA by DNA combing after pulsing cells with CldU and IdU ± RI-1 or B02 (10 μM in each case). Mean ± S.D. of n=3 experiments shown. Error bars in parts **B**-**C** and **E**-**H** represent S.D. of the mean. P values were calculated by one-way ANOVA with Dunnett's multiple comparison test (**B**, **E**, **G**, **H**), unpaired t-test (**C**, **F**), and one-way ANOVA with Tukey's multiple comparison test (**I**). $P < 0.05$ was considered significant.

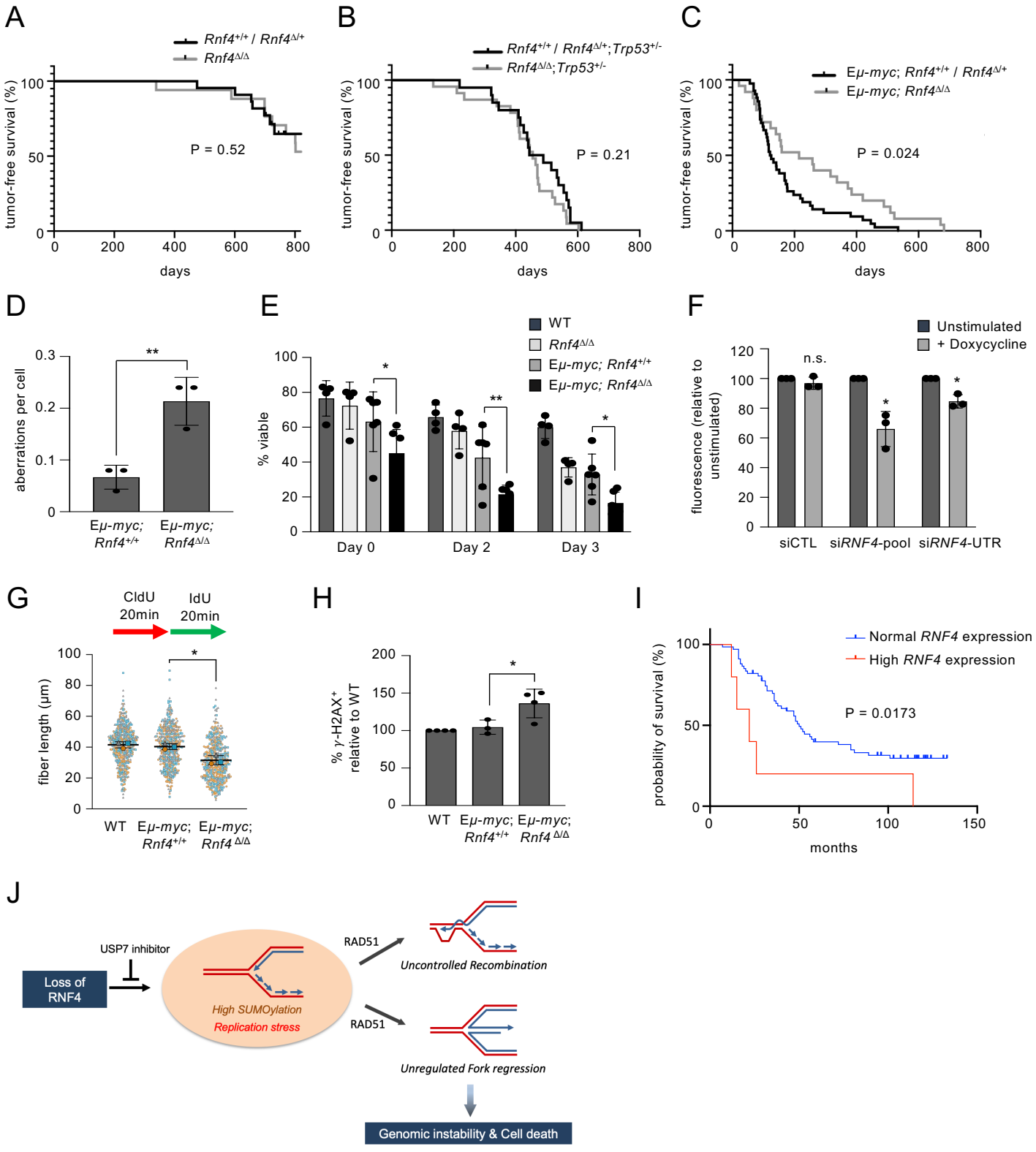

Figure 6: RNF4 deficiency extends tumor-free lifespan of E*μ-myc* transgenic mice. (**A**) Tumor-free survival of *Rnf4*$^{+/+}$;*CD19-Cre* or *Rnf4*$^{f/+}$;*CD19-Cre* (n = 38), and *Rnf4*$^{f/f}$;*CD19-Cre* (n = 44). (**B**) Tumor-free survival of *Rnf4*$^{+/+}$;*Trp53*$^{+/-}$;*CD19-Cre* or *Rnf4*$^{f/+}$;*Trp53*$^{+/-}$;*CD19-Cre* (n = 30), and *Rnf4*$^{f/f}$;*Trp53*$^{+/-}$;*CD19-Cre* (n = 30). (**C**) Tumor-free survival of E*μ-myc*;*Rnf4*$^{+/+}$;*CD19-Cre* or E*μ-myc*;*Rnf4*$^{f/+}$;*CD19-Cre* (n = 47), and E*μ-myc*;*Rnf4*$^{f/f}$;*CD19-Cre* (n = 27). (**D**) Analysis of chromosome aberrations of B cells of the indicated genotypes after two days in culture. (**E**) Analysis of cell viability of B cells of the indicated genotypes during 72 hrs of in vitro growth. (**F**) Growth of U2OS-iMYC cells after doxycycline-induced expression of c-*myc*, measured by quantification of CellTiterGlo fluorescence. P values show difference between the means of unstimulated and stimulated cells. (**G**) Analysis of replication fork velocity measured by DNA combing. Total CldU + IdU tract length is shown. Mean ± S.D. of n=3 experiments shown. (**H**) % of S-phase (EdU^{+}) cells staining positively for γ-H2AX. (**I**) Survival of pediatric B cell acute lymphoblastic leukemia (B-ALL) patients with tumors expressing either normal or increased levels of *RNF4*. (**J**) Model for steps leading to cell death in RNF4-deficient cells. Absence of RNF4 activity causes increased abundance of SUMOylated proteins in chromatin, leading to replication stress and accumulation of non-productive intermediates, dependent on RAD51, which prevents successful completion of DNA replication and further cell proliferation. Error bars in parts **D**-**F**, and **H** show S.D. of the mean. P values were calculated by log-rank test (**A**-**C**, **I**), unpaired t-test (**D**, **F**), two-way ANOVA with Dunnett's multiple comparison test (**E**), and one-way ANOVA with Tukey's multiple comparison test (**G**, **H**). P < 0.05 was considered statistically significant.

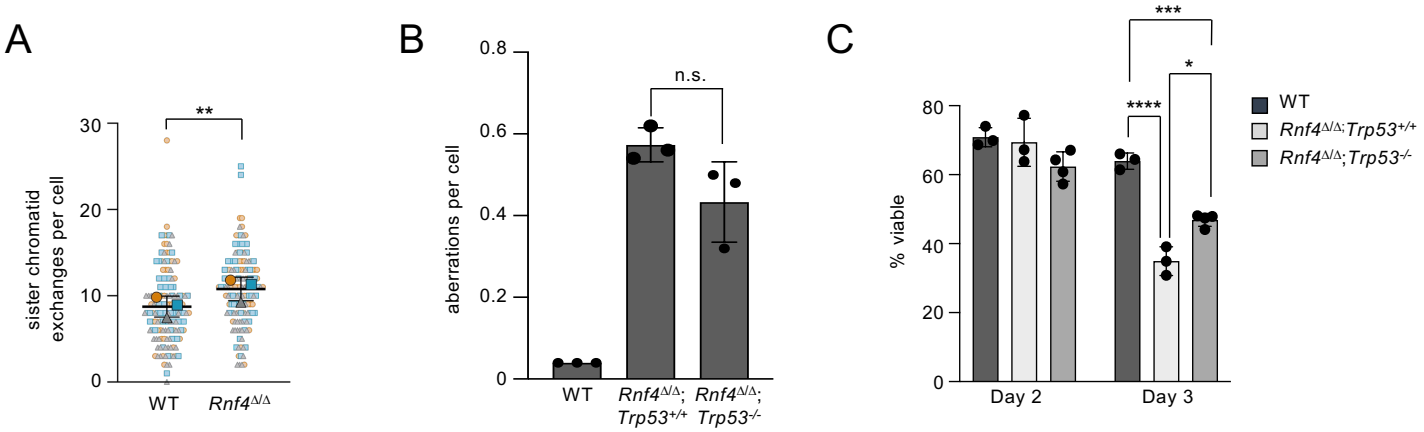

Supplemental Figure 1: (**A**) Quantification of sister chromatid exchanges in WT and *Rnf4*$^{\Delta/\Delta}$ B cells after 48 hrs growth in vitro. Mean ± S.D. of n=3 experiments shown. (**B**) Quantification of metaphase chromosome aberrations from B cells of the indicated genotypes. Error bars show S.D. of the mean. (**C**) Viability of B cells of the indicated genotypes after two or three days in culture. Viable cells were identified by FACS on the basis of PI exclusion. P values were calculated by paired t-test (**A**), unpaired t-test (**B**), and two-way ANOVA with Tukey's multiple comparison test (**C**). $P < 0.05$ was considered significant.

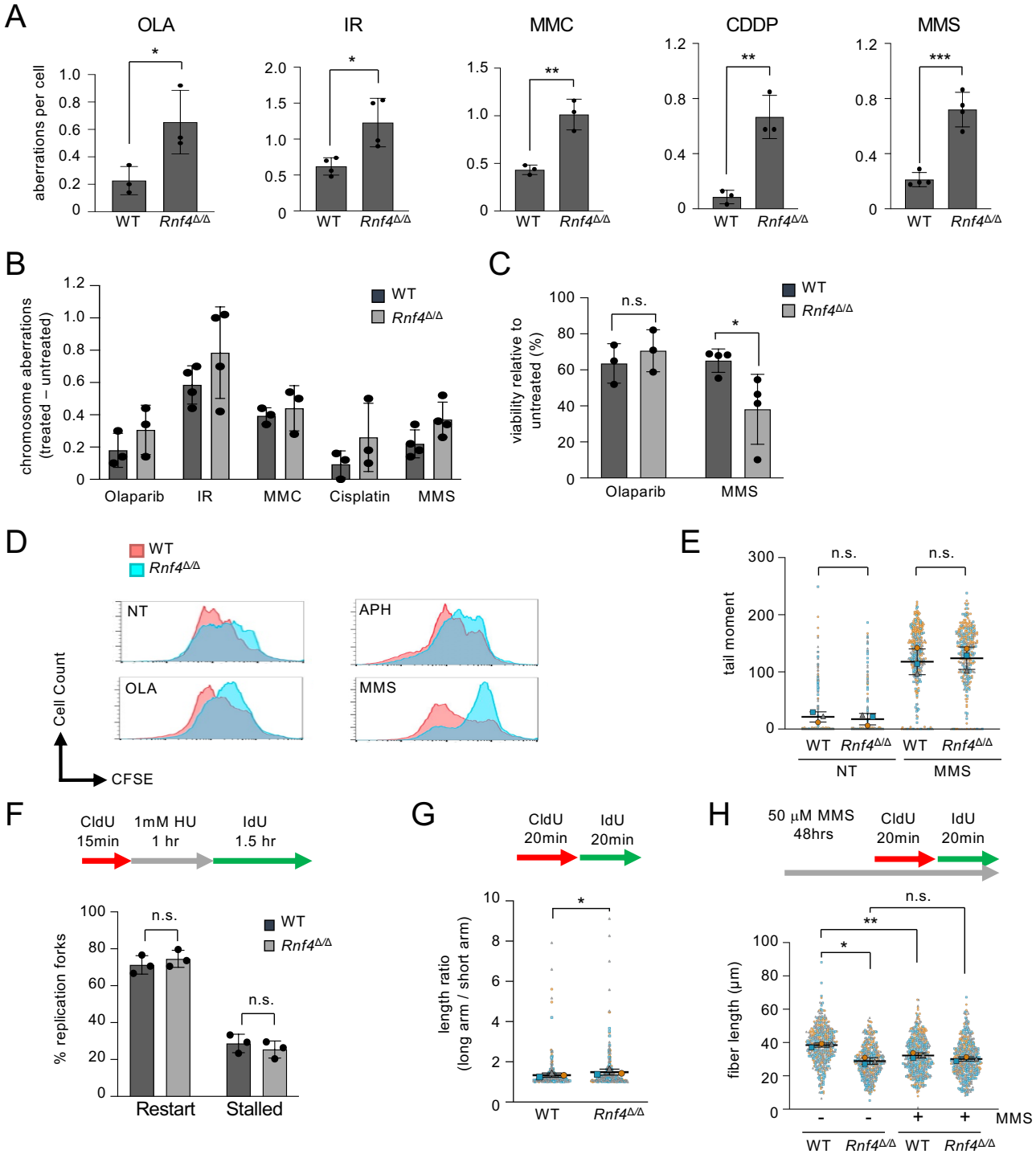

Supplemental Figure 2: (**A**) Chromosome aberrations in WT and *Rnf4*$^{\Delta/\Delta}$ B cells cultured for 36 hrs in vitro followed by overnight treatment with either olaparib (2 μM), ionizing radiation (2 Gy), mitomycin C (MMC, 250 nM), cisplatin (1 μM), or methyl methanesulfonate (MMS, 100 μM). (**B**) Total chromosome aberrations induced by treatments as shown in (A), after subtracting the number of chromosome aberrations present in untreated WT and *Rnf4*$^{\Delta/\Delta}$ B cells. The differences between the means did not meet the threshold for statistical significance ($P < 0.05$) in any case. (**C**) B cell viability after induction of DNA damage. B cells were grown for 72 hrs in culture ± olaparib (1 μM) or MMS (100 μM). Viability was measured by flow cytometry based on DAPI exclusion. (**D**) Representative data for Figure 2B, flow cytometry analysis of CFSE dilution to measure B cell growth in vitro over 72 hrs. (**E**) Alkaline comet assay to measure single-strand DNA breaks in cells of the indicated genotypes after 2 days in culture. MMS treatment was 100 μM, 3 hrs. Mean ± S.D. of n=3 experiments shown. (**F**) DNA fiber analysis to measure fork stalling and restart after hydroxyurea treatment. (**G**) Measurement of asymmetry of replication from single replication origins, measured by DNA fiber analysis. The ratio of the longer replication tract compared to the shorter tract was quantified for each origin. Mean ± S.D. of n=3 experiments shown. (**H**) Measurement of replication fork velocity by DNA combing in untreated cells and after treatment with MMS. Mean ± S.D. of n=3 experiments shown. For parts **A**-**C** and **F**, error bars represent the S.D. of the means. P values were calculated by unpaired t-test (**A**-**C**, **F**), paired t-test (**E**, **G**), and one-way ANOVA with Tukey's multiple comparison test (**H**). $P < 0.05$ was considered statistically significant.

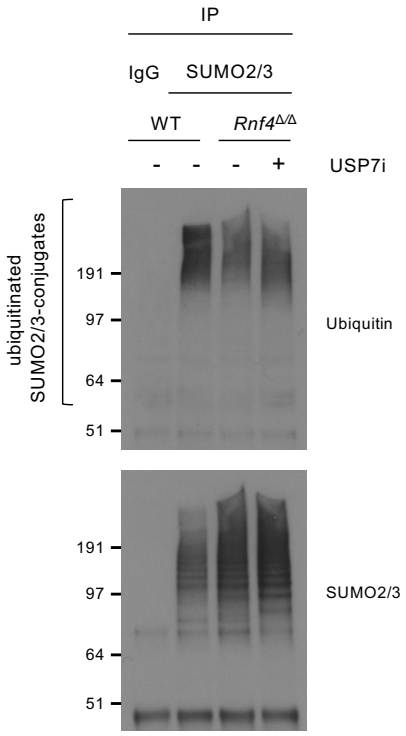

Supplemental Figure 3: Western blot to measure levels of ubiquitination of SUMO-conjugated proteins on chromatin in *Rnf4*$^{\Delta/\Delta}$ B cells after short-term treatment with USP7 inhibitor. B cells cultured in vitro for 48 hrs were either untreated (-) or treated with 50 μM P22077 for 4 hrs. SUMO2/3-conjugates were immunoprecipitated from the chromatin fraction of B cells using an anti-SUMO2/3 antibody, and subsequently used for detection of ubiquitin.

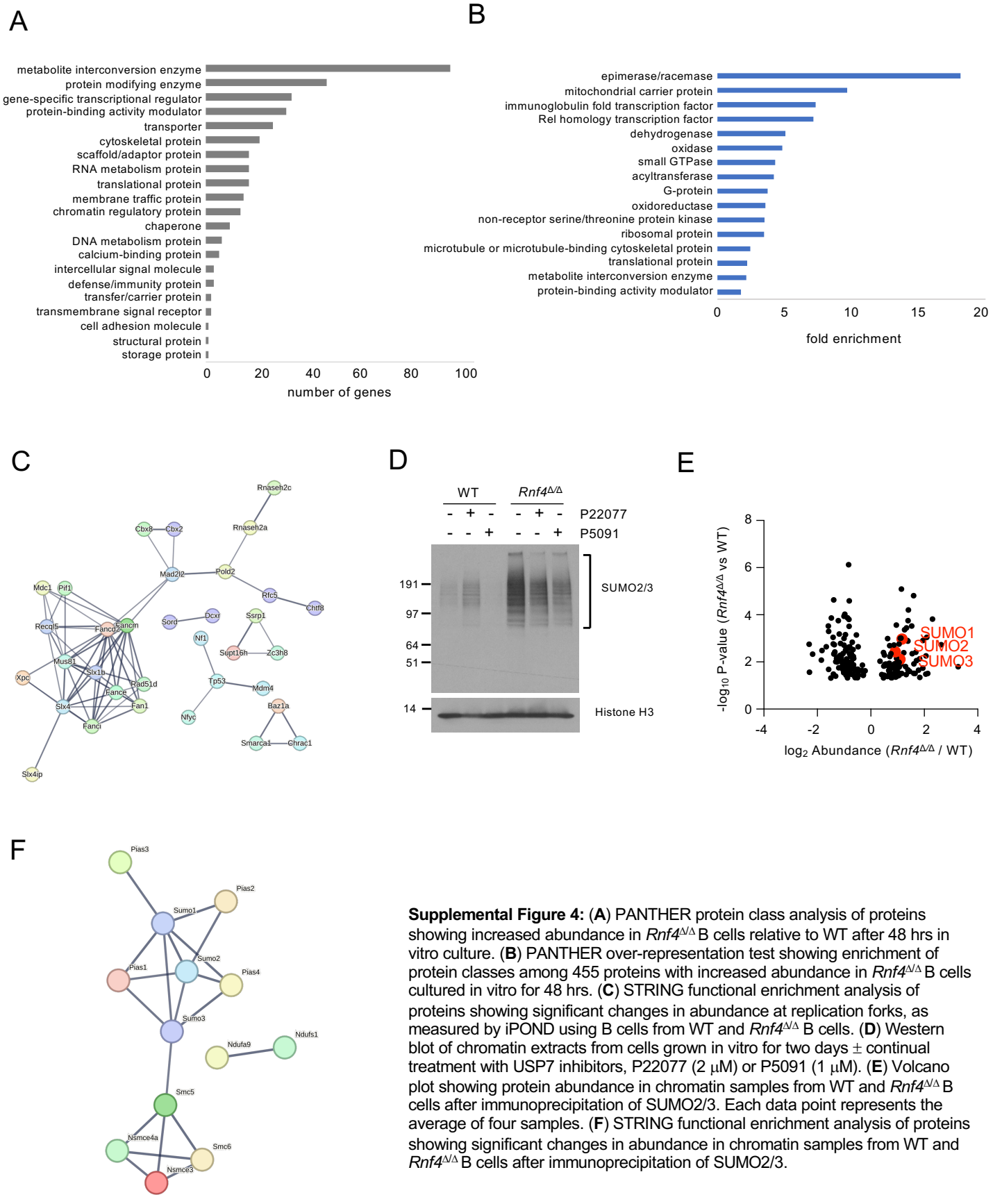

Supplemental Figure 4: (**A**) PANTHER protein class analysis of proteins showing increased abundance in *Rnf4*$^{\Delta/\Delta}$ B cells relative to WT after 48 hrs in vitro culture. (**B**) PANTHER over-representation test showing enrichment of protein classes among 455 proteins with increased abundance in *Rnf4*$^{\Delta/\Delta}$ B cells cultured in vitro for 48 hrs. (**C**) STRING functional enrichment analysis of proteins showing significant changes in abundance at replication forks, as measured by iPOND using B cells from WT and *Rnf4*$^{\Delta/\Delta}$ B cells. (**D**) Western blot of chromatin extracts from cells grown in vitro for two days ± continual treatment with USP7 inhibitors, P22077 (2 μM) or P5091 (1 μM). (**E**) Volcano plot showing protein abundance in chromatin samples from WT and *Rnf4*$^{\Delta/\Delta}$ B cells after immunoprecipitation of SUMO2/3. Each data point represents the average of four samples. (**F**) STRING functional enrichment analysis of proteins showing significant changes in abundance in chromatin samples from WT and *Rnf4*$^{\Delta/\Delta}$ B cells after immunoprecipitation of SUMO2/3.

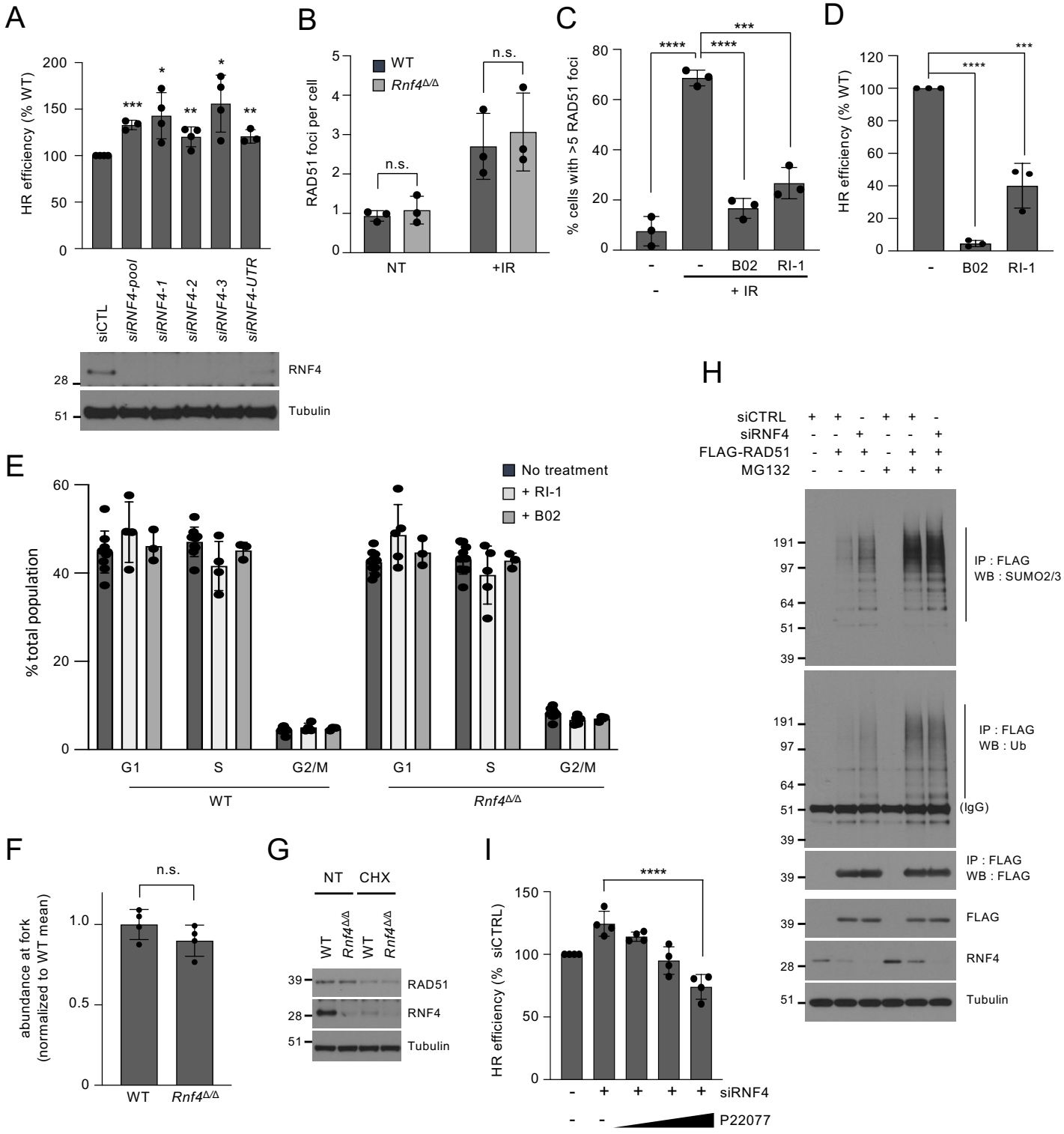

Supplemental Figure 5: (**A**) Measurement of homologous recombination frequency by DR-GFP assay after transfection with either control siRNA (siCTRL) or siRNA oligonucleotides targeting *RNF4*. Efficiency of knockdown is shown by Western blot in the lower panel. (**B**) Quantification of RAD51 foci in cells after no treatment (NT), or after 4 hrs recovery from treatment with 10 Gy of ionizing radiation (IR). (**C**) Analysis of proportion of WT cells showing >5 ionizing radiation-induced nuclear foci after either no treatment (-) or with the RAD51 inhibitors, B02 and RI-1 (1 hr, 50 μM). (**D**) Homologous recombination efficiency measured by DR-GFP assay in cells that were either untreated (-) or treated for 1 hr with B02 (20 μM) or RI-1 (50 μM). (**E**) Measurement of cell cycle by quantification of EdU incorporation and DAPI binding in splenic B cells after 48 hrs growth in vitro ± 10 μM RI-1 or 5 μM B02. (**F**) Abundance of RAD51 at active replication forks, measured by iPOND-MS in n=4 replicate samples. (**G**) RAD51 abundance measured by Western blot in cells that were either not treated (NT) or treated with 25 μg/ml cycloheximide (CHX) for 4 hrs. (**H**) Analysis of ubiquitin present in FLAG-RAD51 pulldown samples in cells treated with either control siRNA (siCTRL) or siRNA targeting RNF4 (siRNF4). Some samples were treated with the proteasome inhibitor, MG132 (10 μM, 4 hrs). (**I**) Homologous recombination efficiency measured by DR-GFP in cells that were treated ± siRNF4 and /or the USP7 inhibitor, P22077 (2, 5, 10μM). Error bars in **A**-**F**, and **I** represent the S.D. of the mean. P values were calculated by unpaired t-test (**A**, **B**, **F**), one-way ANOVA with Tukey's multiple comparison test (**C**, **I**), and one-way ANOVA with Dunnett's multiple comparison test (**D**). $P < 0.05$ was considered significant.

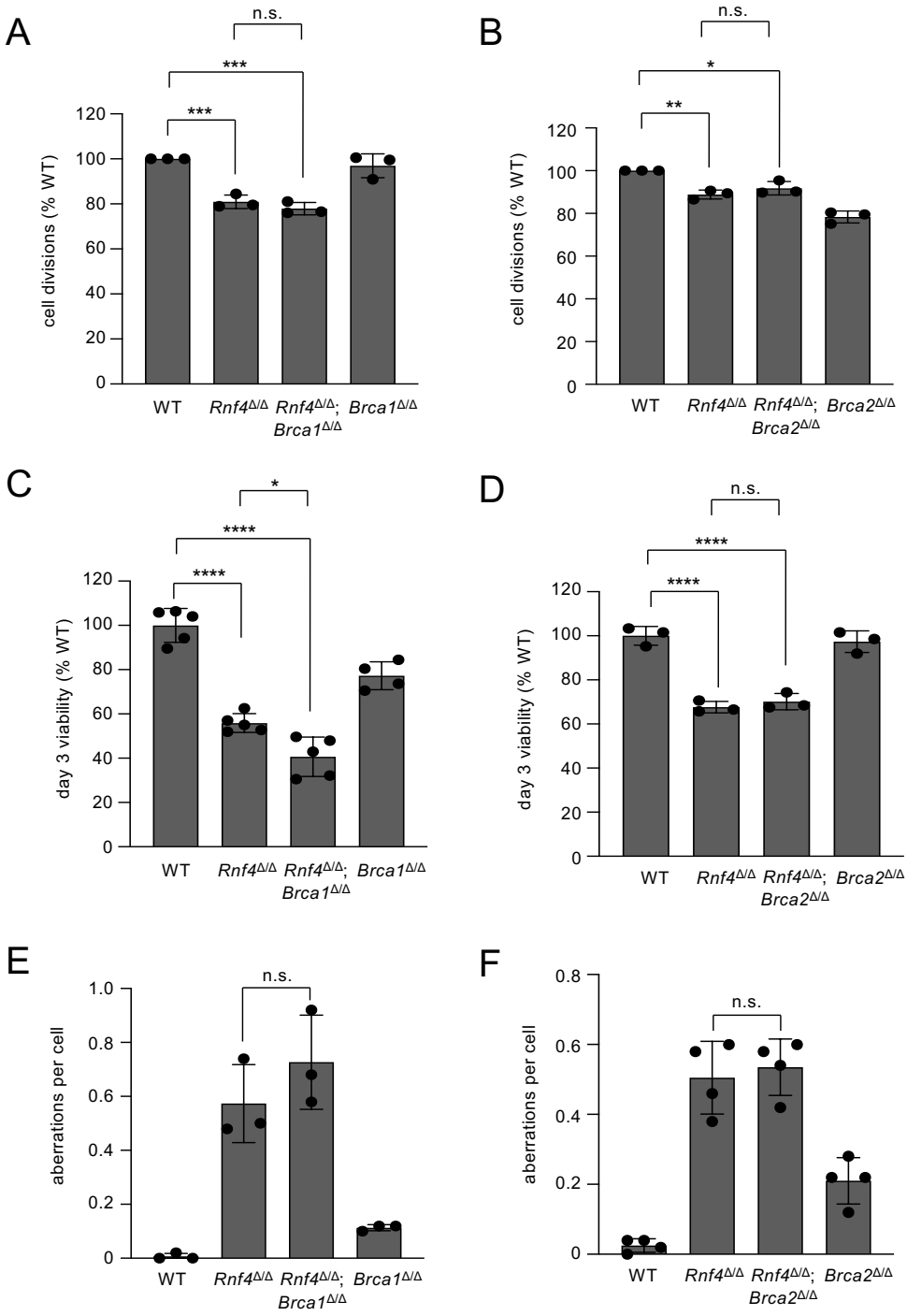

Supplemental Figure 6: (**A**) Quantification of proliferation of B cells growing in vitro for 72 hrs, measured by flow cytometry analysis of CFSE dilution. *Rnf4* and *Brca1* were deleted either singly or in combination in the B cell lineage by breeding to a CD19-Cre transgenic line. (**B**) as (**A**) but with conditional deletion of *Brca2* on a WT or *Rnf4*$^{\Delta/\Delta}$ background. (**C**) Quantification of cell viability of cells of the indicated genotypes, after three days of in vitro B cell culture. Cell viability was measured by DAPI exclusion, as detected by flow cytometry. (**D**) As (**C**) but with deletion of *Brca2*. (**E**) Quantification of chromosome aberrations of B cells of the indicated genotypes. (**F**) As (**E**) but with conditional deletion of *Brca2.* Error bars show the S.D. of the mean in each case, with P values calculated by one-way ANOVA with Tukey's multiple comparison test. A P value < 0.05 was considered statistically significant.

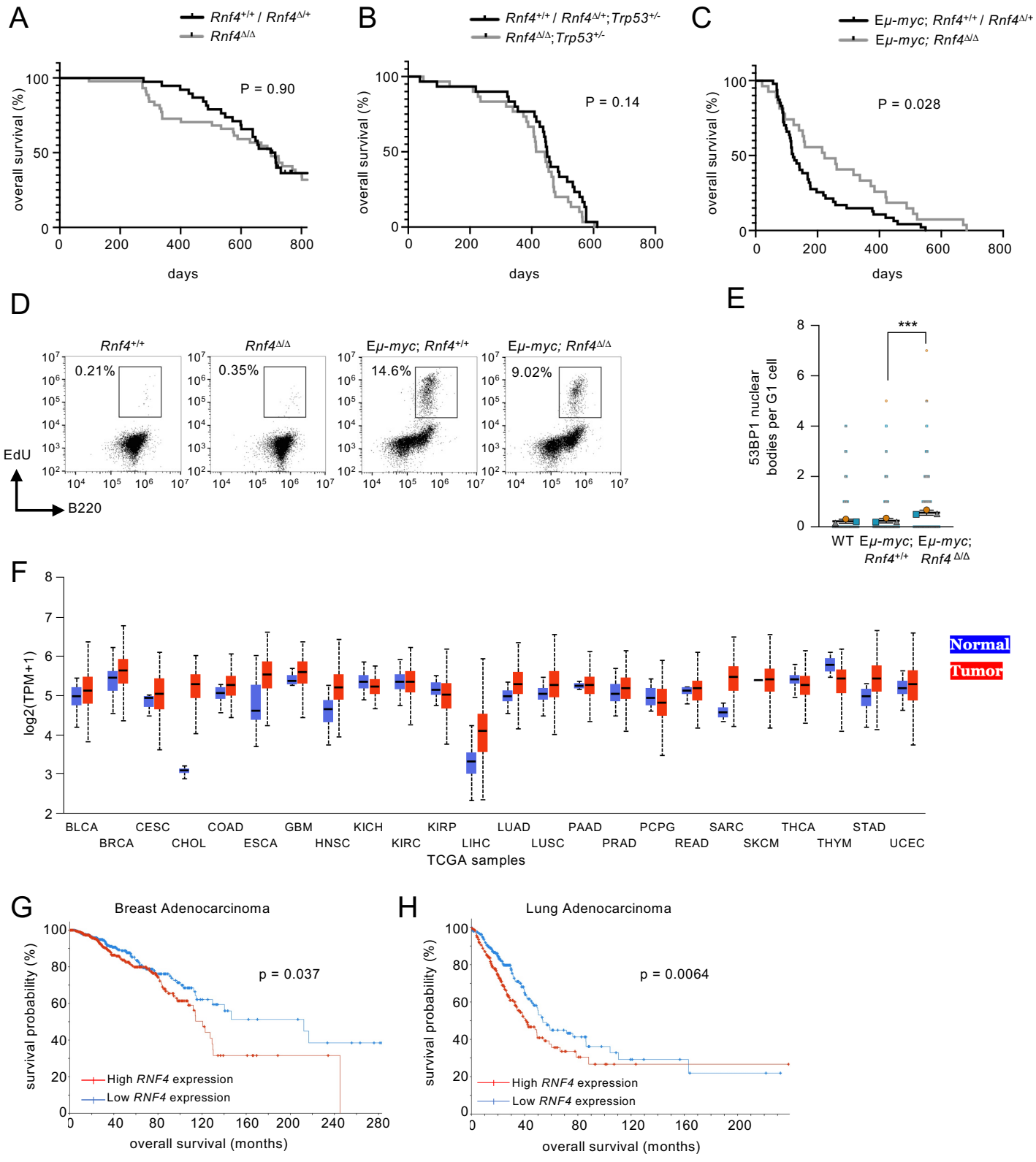

Supplemental Figure 7: (**A**) Kaplan-Meier analysis showing overall survival of *Rnf4*$^{+/+}$;*CD19-Cre* or *Rnf4*$^{f/+}$;*CD19-Cre* (n = 38), and *Rnf4*$^{f/f}$;*CD19-Cre* (n = 44). (**B**) Kaplan-Meier analysis of overall survival of *Rnf4*$^{+/+}$;*Trp53*$^{+/-}$;*CD19-Cre* or *Rnf4*$^{f/+}$;*Trp53*$^{+/-}$;*CD19-Cre* (n = 30), and *Rnf4*$^{f/f}$;*Trp53*$^{+/-}$;*CD19-Cre* (n = 30). (**C**) Kaplan-Meier analysis of overall survival of E*μ-myc*;*Rnf4*$^{+/+}$;*CD19-Cre* or E*μ-myc*;*Rnf4*$^{f/+}$;*CD19-Cre* (n = 47), and E*μ-myc*;*Rnf4*$^{f/f}$;*CD19-Cre* (n = 27). (**D**) Flow cytometry analysis showing EdU uptake by B220^{+} resting B cells from the spleens of WT, *Rnf4*$^{Δ/Δ}$, and E*μ-myc* transgenic mice. (**E**) Quantification of 53BP1 G1 nuclear bodies, measured by anti-53BP1 immunofluorescence in G1 cells of the indicated genotypes after two days of in vitro culture. P value calculated with Mann-Whitney U-test. Mean ± S.D. of n=3 experiments shown. (**F**) Expression of *RNF4* in different tumor types according to TCGA data sets. (**G**) Survival of breast adenocarcinoma patients with tumors expressing either above-median (n = 541) or below-median (n = 541) levels of RNF4. Data from TCGA PanCancer Atlas retrieved through cBioPortal. (**H**) Survival of patients with lung adenocarcinoma expressing either above-median (n = 249) or below-median (n = 252) levels of RNF4. P values in **A**-**C** and **G**-**H** calculated by log-rank test. P value in **E** calculated by paired t-test. P < 0.05 was considered significant in each case.